CHAPTER IV
RESULTS AND DISCUSSION

4.1 Selective Oxidation of Ethylene over Ag on High Surface Alumina Catalysts

4.1.1 Characterization Results

Oxygen TPD profiles for various Ag loadings are shown in Figure 4.1 There was a sole desorption peak for each catalyst at around 250 – 300°C. The position of the TPD peak maximum shifted to slightly higher temperatures with increasing silver loading and reached a maximum value of 306°C for the 13.18% Ag/Al_2O_3 catalyst. The desorption curves show the onset of a broad additional desorption feature beyond 450°C. The first peak at around 250 – 300°C can be attributed to the decomposition of bulk Ag_2O to metallic Ag. The other peaks starting at 450°C and extending to higher temperatures beyond 600°C may be due to the decomposition of the dispersed Ag_2O phase, which is more stable than bulk phase Ag_2O (Luo *et al.*, 1998). It was noticed that the amount of O_2 desorption for 13.18% Ag/Al_2O_3 was higher than for other silver loadings. This suggests 13.18%

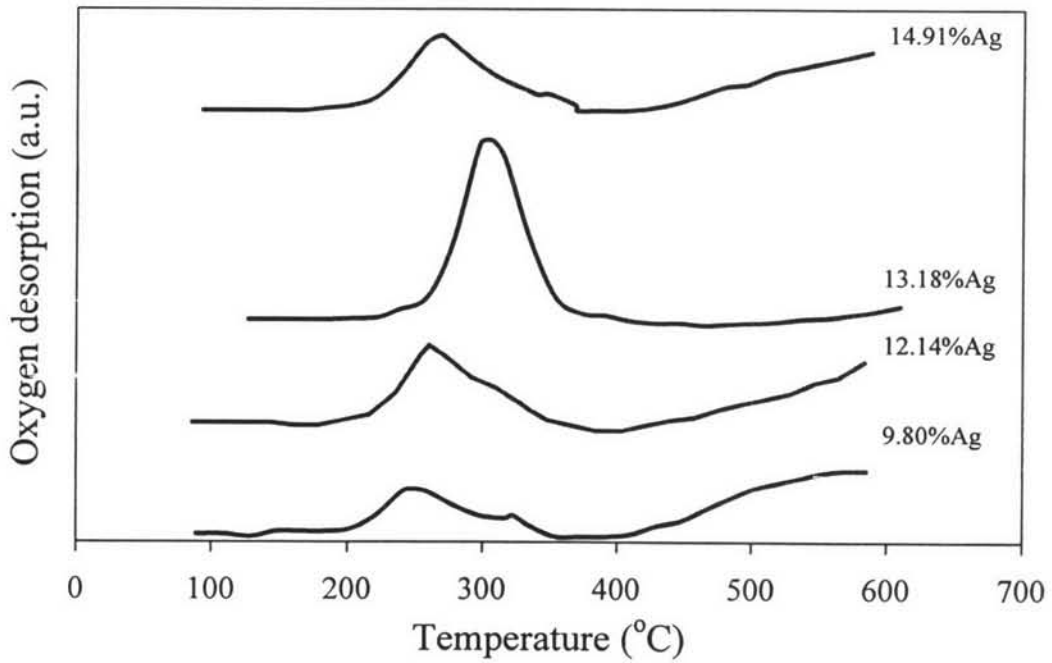

Figure 4.1 TPD profiles of O2 of the Ag/Al_2O_3 at various silver loadings.

Ag/Al_2O_3 catalyst has the largest number of active silver surface sites capable to adsorb by oxygen. This is confirmed by XPS results as shown in Table 4.1 where the 13.18% Ag/Al_2O_3 has the highest AgO/Ag ratio obtained the highest ratio's value (1.83). However, for the starting condition of XPS, the catalyst sample was fresh, while the condition of TPD experiment was started by exposure with O_2, therefore; the AgO/Ag ratio after O_2 exposure should be higher. Thus, it showed the highest TPD profiles.

Table 4.1 The AgO/Ag ratios of Ag catalysts at different Ag loadings (from Ag $3d_5$ and $Ag3d_3$ of XPS)

Catalysts	AgO/Ag Ratio
9.80% Ag/Al_2O_3	1.51
12.14% Ag/Al_2O_3	1.62
13.18% Ag/Al_2O_3	1.83
14.91%Ag/Al_2O_3	1.34

Moreover, the XPS binding energy (BE) for each peak were nearly the same for the entire series of catalysts. The Ag $3d_3$ binding energy was in the range of 373.86 - 374.85 eV, corresponding to the characteristic for the metallic state of silver (374.2 eV). The Ag $3d_5$ binding energy of 367.78-368.61 eV can be attributed to AgO (367.7 eV), and Ag and Ag_2O (368.2 eV). The O 1s peak (530.87-531.74 eV) corresponds to O 1s (531.1 eV) in the alumina support, in agreement with the Al 2p peak position. (72.9 eV) corresponding to Al_2O_3 [www.xpsdata.com].

The XRD patterns of catalysts with various silver loadings (Figure 4.2) display 4 dominant peaks at $2\theta = 38°$ and 77° representing for metallic silver, and at $2\theta = 44°$,and 64° representing for silver oxide and metallic silver. These peaks reached higher intensity with increasing silver loading. The results indicate that all silver catalysts contain both metallic silver and silver oxide. The mean crystallite size was calculated from the Scherrer equation as shown in Table 4.2. As be seen in table, the calculated values of the mean crystallite sizes of the catalysts are in the range of 180-190 Å.

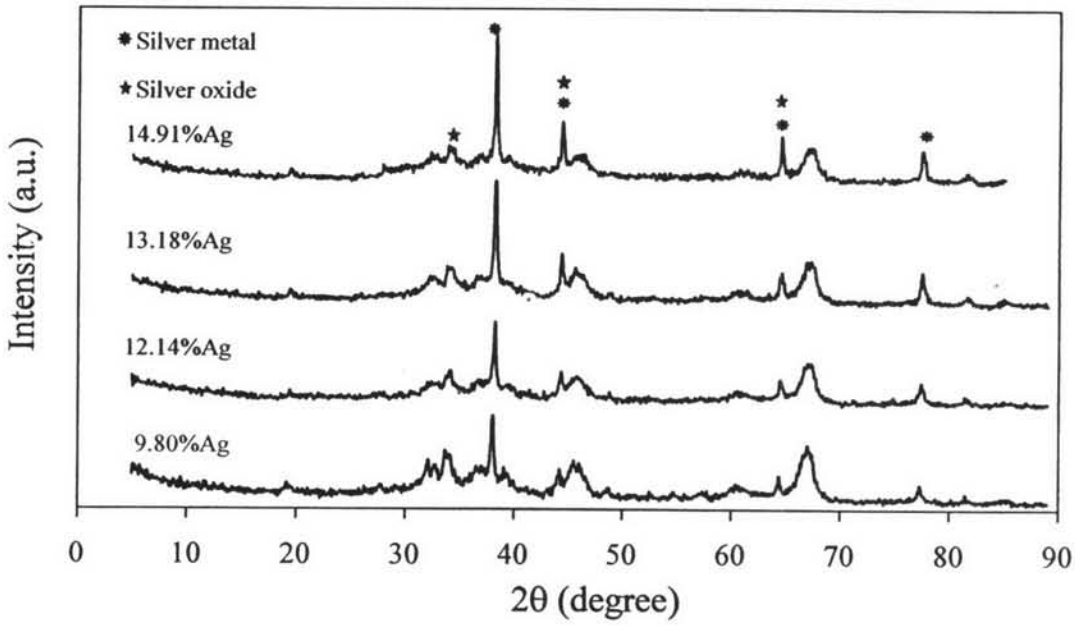

Figure 4.2 XRD patterns of the Ag/Al_2O_3 catalysts at various silver loadings.

Table 4.2 Mean crystallite sizes of silver catalysts at various silver loadings

Catalysts	Mean crystallite size, Å
9.80% Ag/Al_2O_3	180
12.14% Ag/Al_2O_3	189
13.18% Ag/Al_2O_3	192
14.91%Ag/Al_2O_3	183

STEM equipped with EDS can be used to identify the elemental composition of individual particles of a catalyst. Figure 4.3 shows transmission electron micrographs of the 13.18% Ag/Al_2O_3 catalyst. Figure 4.3 (a) shows many high contrast particles and many of them are agglomerated into aggregated particles. Figure 4.3 (b) shows a close-up image of an area containing particles of both silver as well as silver oxide dispersed on the support. For example, when the electron

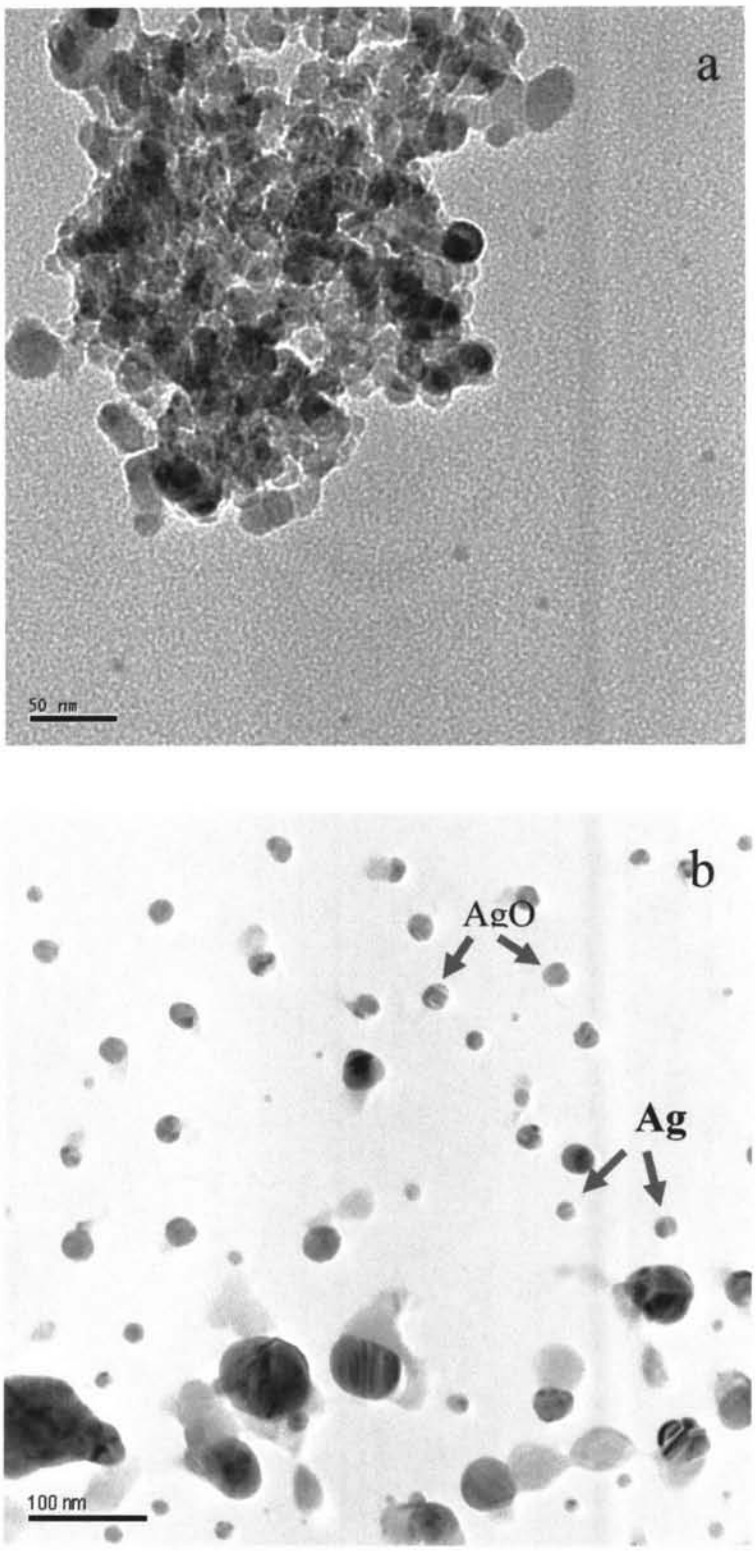

Figure 4.3 STEM micrographs of 13.18% Ag/Al_2O_3: (a) aggregates of silver and silver oxide; (b) individual Ag and AgO particles.

beam was stopped over one individual particle whose particle size was around 210 Å, the EDS analysis revealed that this particle contained only metallic silver. A somewhat larger particle with about 300 Å in diameter, on the other hand, gave EDS signals for both silver as well as oxygen, indicating that this particle consists of AgO. From the micrographs, it is apparent that there is a wide range of particle sizes. Some of the very large particles observed are significantly larger than the average particle size calculated from XRD line broadening. The reason for this discrepancy is that XRD actually measures the size of microcrystalline domains; while the regions of high contrast visible in a STEM micrograph may encompass particles containing several microcrystalline domains.

4.1.2 Catalyst Activity for Epoxidation of Ethylene

The ethylene epoxidation experiments were carried out at different temperatures. For each operational temperature, the reaction was allowed to continue until it came to steady state before taking data. Figure 4.4 shows ethylene conversion increases with increasing temperature, while selectivity of ethylene oxide decreases drastically with increasing temperature (Figure 4.5). It can be simply concluded that a higher temperatures favor the complete oxidation over the partial oxidation. Within the Ag loading range studied, it was noticed that at any given temperature, the ethylene oxide selectivity increased with increasing Ag loadings and reached a maximum at 13.18% Ag/Al_2O_3. From the characterization results, it also appears that this catalyst has the largest crystallite size (Table 4.2) and AgO/Ag ratio (from XPS, Table 4.1). Therefore, this fumed alumina support can facilitate the formation of large Ag particles which are according to STEM either metallic Ag with average size of 210 Å , or AgO with average size of 300Å. Wu *et al.* (Wu and Harriott, 1975) found that catalysts with Ag particle size less than 20 Å showed nearly zero ethylene oxide selectivity, and the selectivity improved with increasing particle size up to 1000 Å. Thus, it can be stated that ethylene epoxidation depends more on the particle size than on the interaction between Ag and the Al_2O_3 support. Moreover, a high ratio of AgO/Ag of catalyst showed better performance because in the presence of AgO can suppress the dissociation of molecular oxygen on silver surface. The reason is that if no vacant neighboring adsorption sites are available,

molecularly adsorbed oxygen will not dissociate and may remain molecularly adsorbed to high temperatures (Ertl *et al.*, 1997). From the TPD result, the 13.18% Ag/Al_2O_3 catalyst provides the maximum oxygen coverage than others; therefore, ethylene epoxidation is maximized. van Santen and his group (Ertl *et al.*, 1997) demonstrated that maximum oxygen coverage obtainable had a stoichiometry of one oxygen adatom to one surface silver, as in AgO, located in subsurface position. The presence of subsurface oxygen atoms will reduce the electron density on neighboring silver atoms. When contact with an alkene, the interaction between ethylene π electrons and oxygen electrons will lead to a flow of oxygen electrons to the positive charged surface metal atoms. Surface oxygen adatoms then behave as electrophilic oxygen atoms that preferentially react with high electron density part of molecule, as the π bond of ethylene as shown in Figure 4.7. Based on the results show in Figure 4.5 and 4.6, the optimum temperature is around 240°C giving around 80% for the ethylene oxide selectivity and around 2% for the ethylene oxide yield. Mao and his groups (Mao and Vannice, 1995a and 1995b) studied the high surface area α–Al_2O_3 and found that it gave non ethylene oxide selectivity. The reason is that their catalysts contained very small Ag particles with around 2-3 nm, which are considerably too small to promote ethylene epoxidation.

The effects of concentration ratio of C_2H_4:O_2 on the ethylene oxide selectivity and yield are shown in Figures 4.8-4.9. Due to a very low conversion of ethylene, oxygen material balance was applied to calculate ethylene oxide product. Figure 4.8 shows that the concentration ratio of C_2H_4:O_2 of 6%:6% provides the highest ethylene oxide selectivity, while the concentration ratio of C_2H_4:O_2 of 10%:10% exhibits the highest yield (Figure 4.9). As be known, the ethylene oxide reaction requires a high oxygen surface coverage on the silver surface (Ertl *et al.*, 1997); therefore, the 10% to 10% ratio provides the highest oxygen coverage resulting in the highest yield as compared to the other concentration ratios having lower oxygen concentrations.

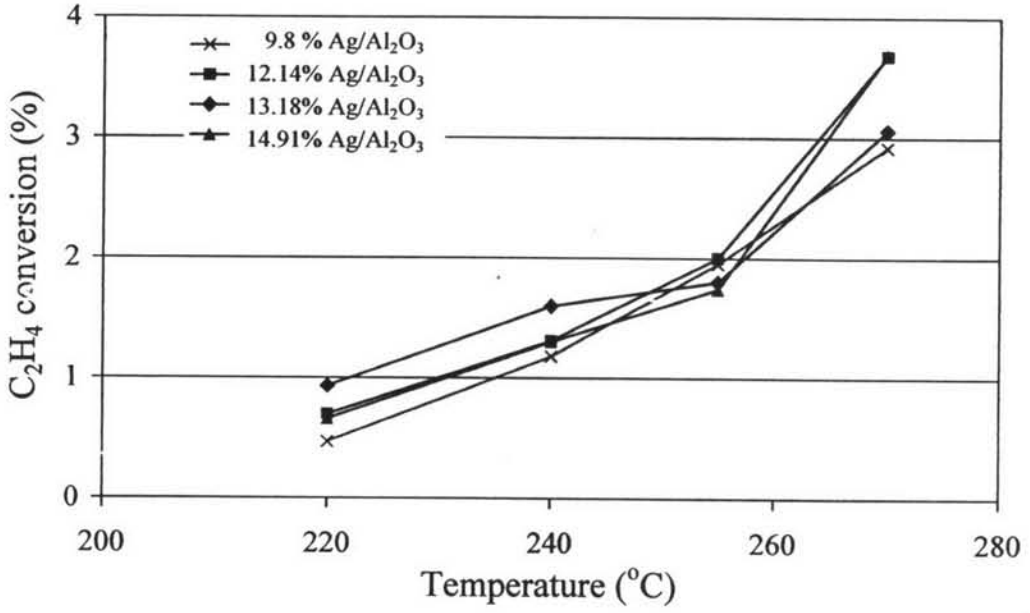

Figure 4.4 Ethylene conversion at various silver loadings at space velocity of 6,000 h^{-1}, P = 10 psig and 6% O_2 and 6% C_2H_4 balance with He.

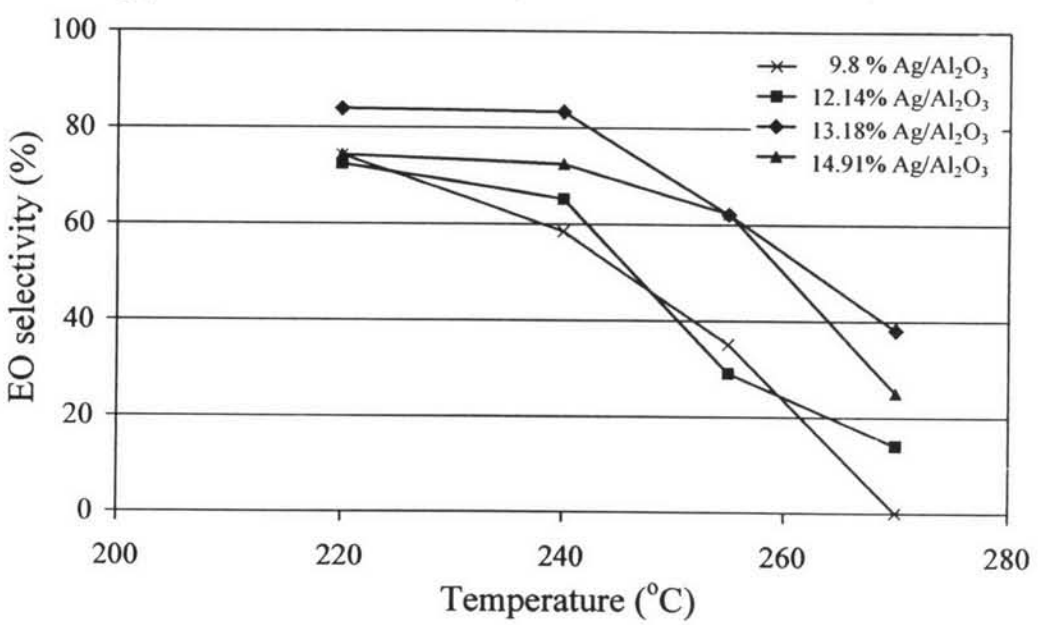

Figure 4.5 Ethylene oxide selectivity at various silver loadings at space velocity of 6,000 h^{-1}, P = 10 psig and 6% O_2 and 6% C_2H_4 balance with He.

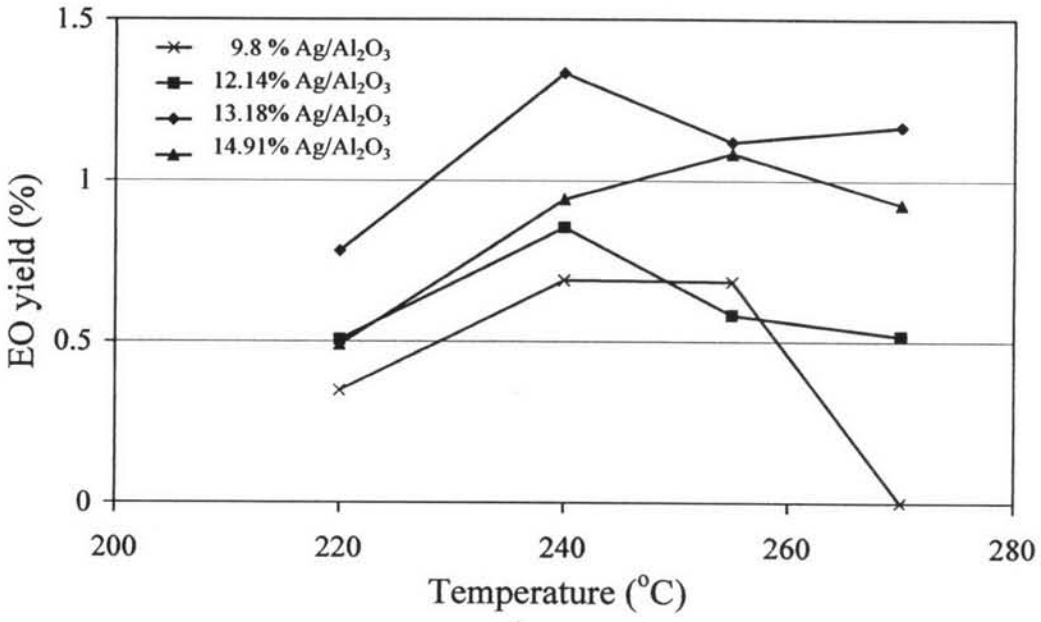

Figure 4.6 Ethylene oxide yield at various silver loadings at space velocity of 6,000 h^{-1}, P = 10 psig and 6% O_2 and 6% C_2H_4 balance with He.

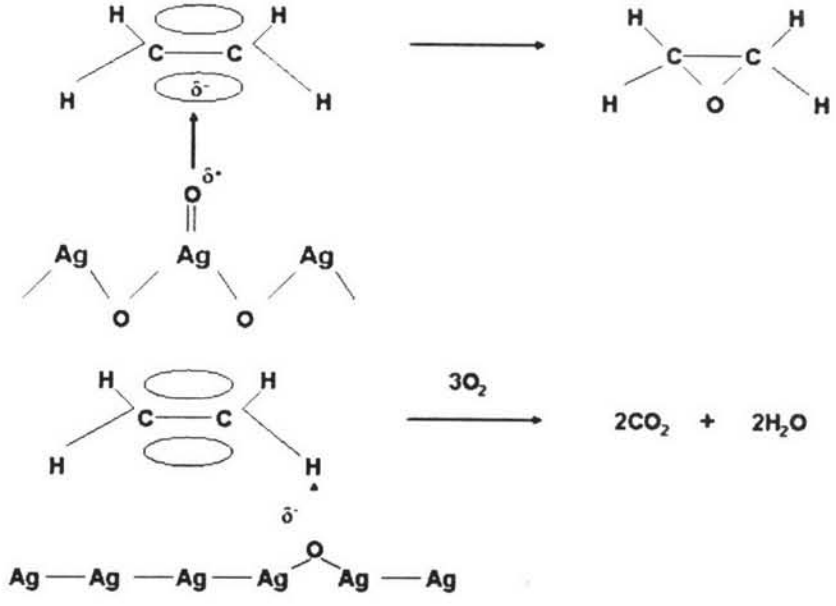

Figure 4.7 Schematic representation of the surface conditions that lead to epoxidation (Ertl *et al.*, 1997).

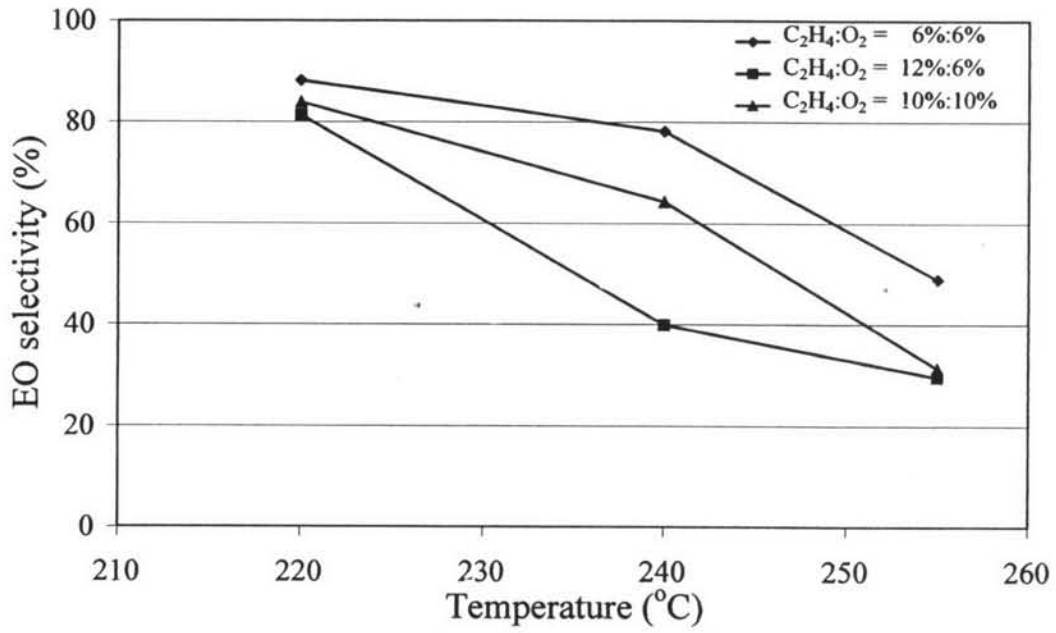

Figure 4.8 Ethylene oxide selectivity at 13.18% Ag/Al_2O_3 with space velocity of 6,000 h^{-1}, P = 10 psig at various concentration ratio of C_2H_4:O_2.

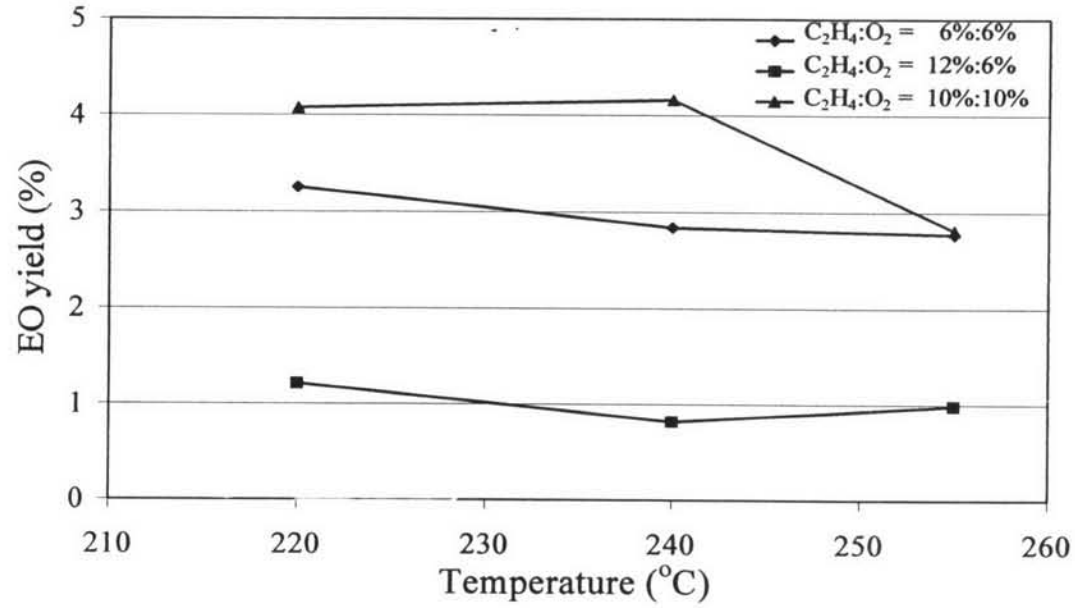

Figure 4.9 Ethylene oxide yield at 13.18% Ag/Al_2O_3 with space velocity of 6,000 h^{-1}, P = 10 psig at various concentration ratios of C_2H_4:O_2.

The presence of ethylene oxide was confirmed by the subsequence reaction detected with mass spectrometry (as shown in Appendix A, Figure A.1). With this technique, the result showed the trend of ethylene oxide presence, but it was not absolutely clear. Therefore, DRIFTS reaction was employed to prove ethylene oxide produced over the catalyst. The procedure of DRIFTS experiment was well described in chapter III. The reaction over the 13.18% Ag on Al_2O_3 catalyst was done at 220°C. The FT-IR spectrum presented was collected after 30 min with continuous flow to ensure steady state reaction. Figure 4.10 shows comparatively the spectra of bulk gas over the catalyst and the two standard spectra of pure ethylene and ethylene oxide. Comparing to a library's information, two spectra were attributed to epoxy ring (800-1300 cm^{-1}) and CH-bend (1300-1600 cm^{-1}) (Skoog *et al.*, 1998). In addition, two bands of CO_2 at 2317 and 2360 cm^{-1} also were found. From the DRIFTS results, the formation of ethylene oxide over the studied catalyst was confirmed.

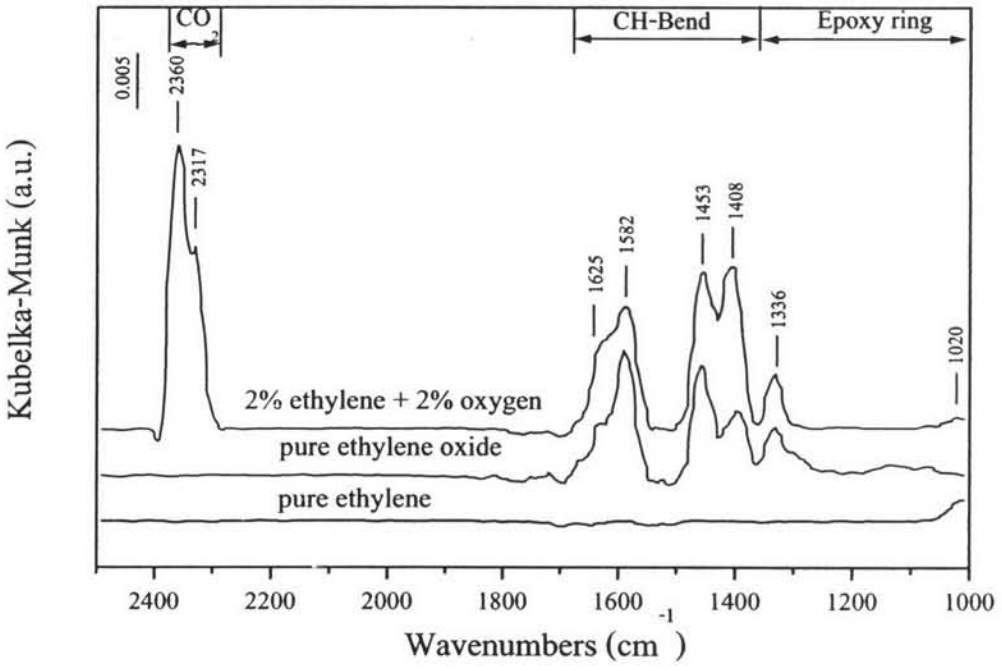

Figure 4.10 DRIFTS spectrum over 13.18% Ag/Al2O3 after 30 min exposure time.

4.1.3 Conclusions

The TPD profiles of oxygen showed a slight shift of the maximum deposition peak towards higher temperatures with increasing silver loadings. The corresponding temperature for the TPD peak maximum reached the highest value for the 13.18% Ag/Al_2O_3, followed by a decrease to lower peak temperatures with further increase in Ag loading. The desorption peaks can be ascribed to the decomposition of Ag_2O to metallic Ag. The catalyst that showed the highest selectivity and yield of ethylene oxide gave the highest desorption peak temperature, suggesting that in this catalyst the AgO phase is more stable. There is no clear trend in particle size as a function of silver loading. Analytical electron microscopy revealed the presence of both metallic Ag and AgO particles. In general, the AgO particles tend to be larger than the metallic Ag particles. The average particle size calculated from XRD is smaller than the STEM derived average particle size. This may indicate that some of the particles contain more than one microcrystalline domain. From the experimental reaction results, it was found that 13.18% Ag/Al_2O_3, which provided the largest crystallite size, gave the highest conversion of ethylene and selectivity and yield of ethylene oxide. It was a good correlation between crystallite size and the activity study that this high surface alumina provided suitable Ag particle size enhanced the ethylene epoxidation. Moreover, silver on high surface alumina prevented sintering effect due to high dispersion of silver. In addition, the effect of oxygen coverage on silver active site showed that high oxygen coverage as $C_2H_4:O_2$ = 10%:10% enhanced the ethylene oxide production.

4.2 Selective Oxidation of Ethylene over Alumina supported Bimetallic Ag-Au Catalysts

Gold is unique among metallic elements because of its resistance to oxidation and corrosion. In addition to its inert character, gold has very low affinity for gas adsorption. However, there is evidence that under certain conditions oxygen can adsorb on gold. For example (MacDonald and Hayes, 1970), when gold powder was exposed to molecular oxygen, oxygen uptake was observed over a wide temperature range with two distinct maxima at -50°C and 200°C, respectively. Adding gold into silver catalysts was found three adsorbed oxygen of atomic oxygen, molecular oxygen and subsurface oxygen at elevated temperatures and showed that alloying Ag with Au influenced the bond strengths with silver surface and modified the relative population of the adsorbed species (Kondarides *et al.*, 1996). In this work, a small amount of gold was added as a promoter in sequence on silver catalyst and to study the effect of gold on the ethylene epoxidation.

4.2.1 Characterization Results

The effects of gold loading on TPD of O_2 were observed for the two experimental protocols, which are with and without a cooling step prior to TPD. Figure 4.11 shows TPD of O_2 after cooling to room temperature. There were no significant differences in the oxygen desorption temperature for catalysts with different gold loadings. There was no maximum desorption peak observed for blank alumina and the 0.79% Au/Al_2O_3 catalyst. This indicates that there are no measurable amounts of oxygen adsorbed on the alumina support and on pure gold supported on alumina. This was in marked contrast to the results of the desorption experiment without a cooling step. As shown in Figure 4.12, there is now a slight shift of the TPD peak maximum toward lower temperatures with increasing gold loading. For example, TPD of O_2 was shifted from 327°C (0.0% Au-13.18% Ag/Al_2O_3) to 308°C (0.93% Au-13.18% Ag/Al_2O_3). This indicates that the interaction between silver and oxygen is weakened in the presence of gold. This is in agreement with the observation of Kondarides and Verykios (1996) who reported a decrease of the heat of adsorption of oxygen with increasing Au content of supported

Ag-Au alloy catalysts. Toreis and Verykios (1987) and Kondarides and Verykios, (1996) explained their results in terms of electronic effects, where the electronic structure of silver atoms has been affected by nearest-neighbor gold atoms. They suggested that d-electrons of gold are transferred to silver and that this transfer is partially compensated by transfer of conducting s, p-electrons in the opposite direction, whereas the dissociative adsorption of oxygen on silver also requires transfer of electrons from silver to oxygen. It is expected that the electron deficiency due to neighbor interaction of gold atoms results in weakening of Ag-O bonds. Thus, the adsorbed species tend to desorb at lower temperatures. When comparing the two cases with and without a cooling step preceding desorption, it becomes apparent that desorption without a cooling step gives peak temperatures 10-20°C lower than in experiments with a cooling step. In TPD of O_2 of 0.79% Au/Al_2O_3 without a cooling step, small oxygen desorption peak is observed. It can be concluded that a small amount of oxygen can adsorb on supported gold at 200°C, but these adsorbed species are unstable when the sample is cooled to room temperature, as there was no TPD peak observed after the cooling step. This observation is in agreement with prior reports of oxygen adsorption on supported Au (Schwank, 1983 and references cited therein).

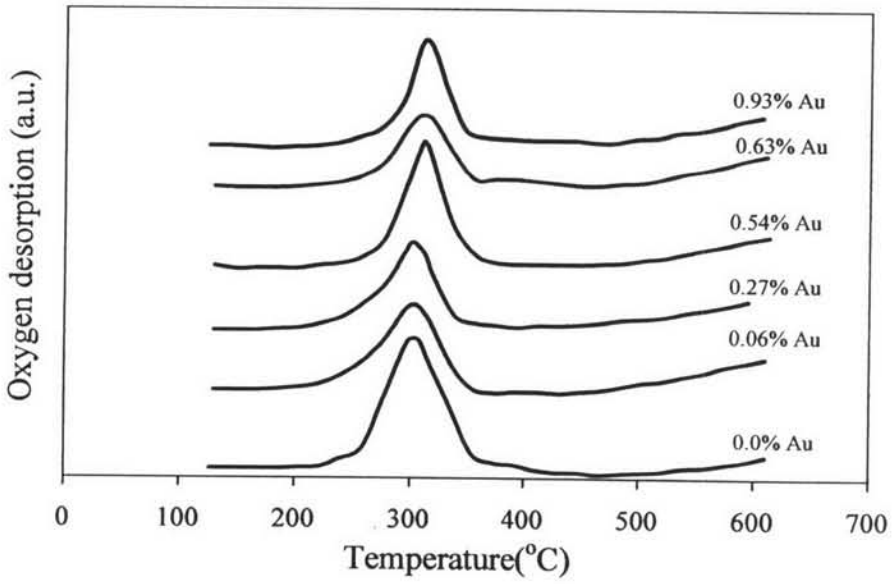

Figure 4.11 TPD profiles of O_2 with cooling step at room temperature of 13.18% Ag/Al_2O_3 at various gold loadings.

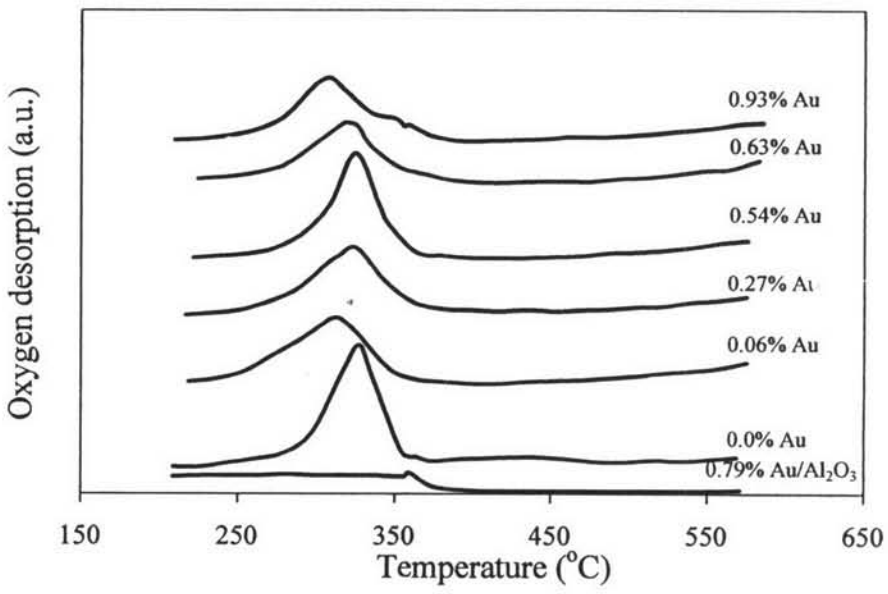

Figure 4.12 TPD profiles of O_2 without cooling step at room temperature of 13.18% Ag/Al_2O_3 at various gold loadings and 0.79% Au/Al_2O_3.

Figure 4.13 (a) shows XRD patterns of 13.18% Ag/Al_2O_3 with various gold loadings of 0.06, 0.27, 0.54, 0.63, and 0.93%. Silver and gold both are face-centered cubic metals and the atomic radii of the two elements are quite similar (1.444 Å for silver and 1.441 Å for gold). Given the relatively small amount of gold, the gold peaks cannot be clearly resolved from the silver peaks. The effect of gold on XRD patterns become more pronounced at higher gold loadings. Figure 4.13 (b) shows a close-up of the (111) peak region. In two of the catalysts, namely the 0.54% wt Au, and the 0.93% Au samples, the (111) peaks are noticeably shifted to higher values. These shifts in XRD peak position indicate an interaction between Ag and Au, resulting in a quite significant decrease in lattice constant to a value of 4.0795 Å, compared to 4.0884 Å for the monometallic Ag sample. The theoretical lattice constants calculated from the atomic radius of silver and gold at room temperature are 4.085438 Å for Ag and 4.08453Å for gold. The (311) peak region (Figure 4.13 (c)) shows significant differences in both peak shape and position not only for the 0.54% Au and the 0.93 % Au samples, but also for the 0.63% Au sample. This leads further support to the notion that there is an interaction between Ag and Au, causing the lattice to contract. Figure 4.13 (d) shows how the lattice constants determined

from the peak positions for the (111) and (311) planes change as a function of gold content.

The mean crystallite size was calculated from XRD data by using the Scherrer equation. Due to the overlapping of the silver and gold peaks, we cannot calculate crystallite sizes of gold and silver separately. The mean crystallite size of the Ag-Au catalysts was in the range of 180-186 Å (Table 4.3). Gold addition did not appear to significantly affect the particle size.

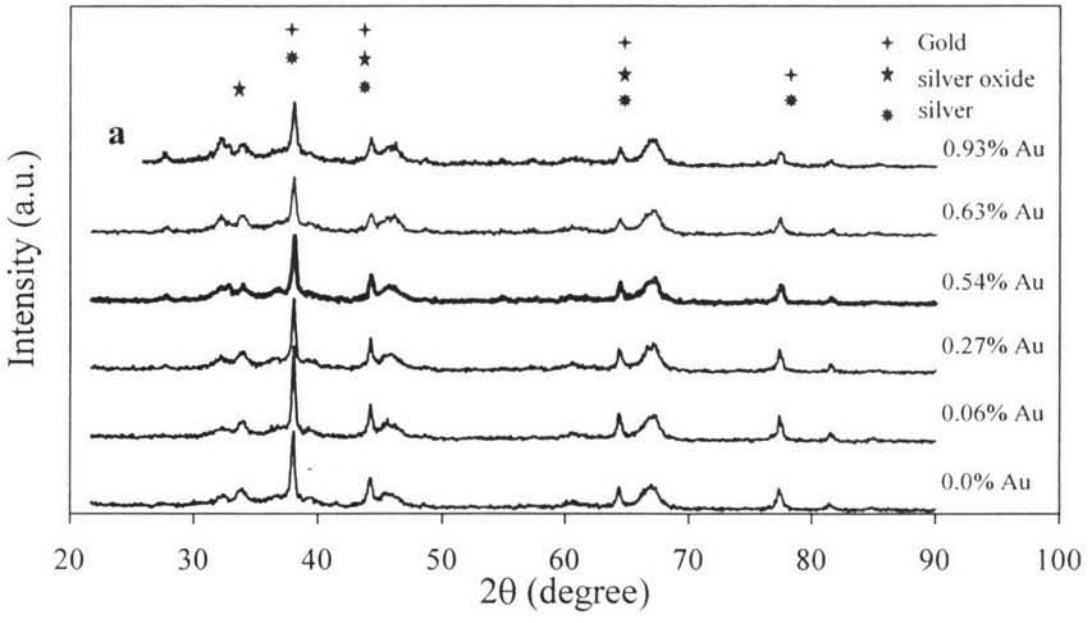

Figure 4.13 XRD patterns of 13.18% Ag/Al_2O_3 at various gold loadings:
(a) overview patterns;

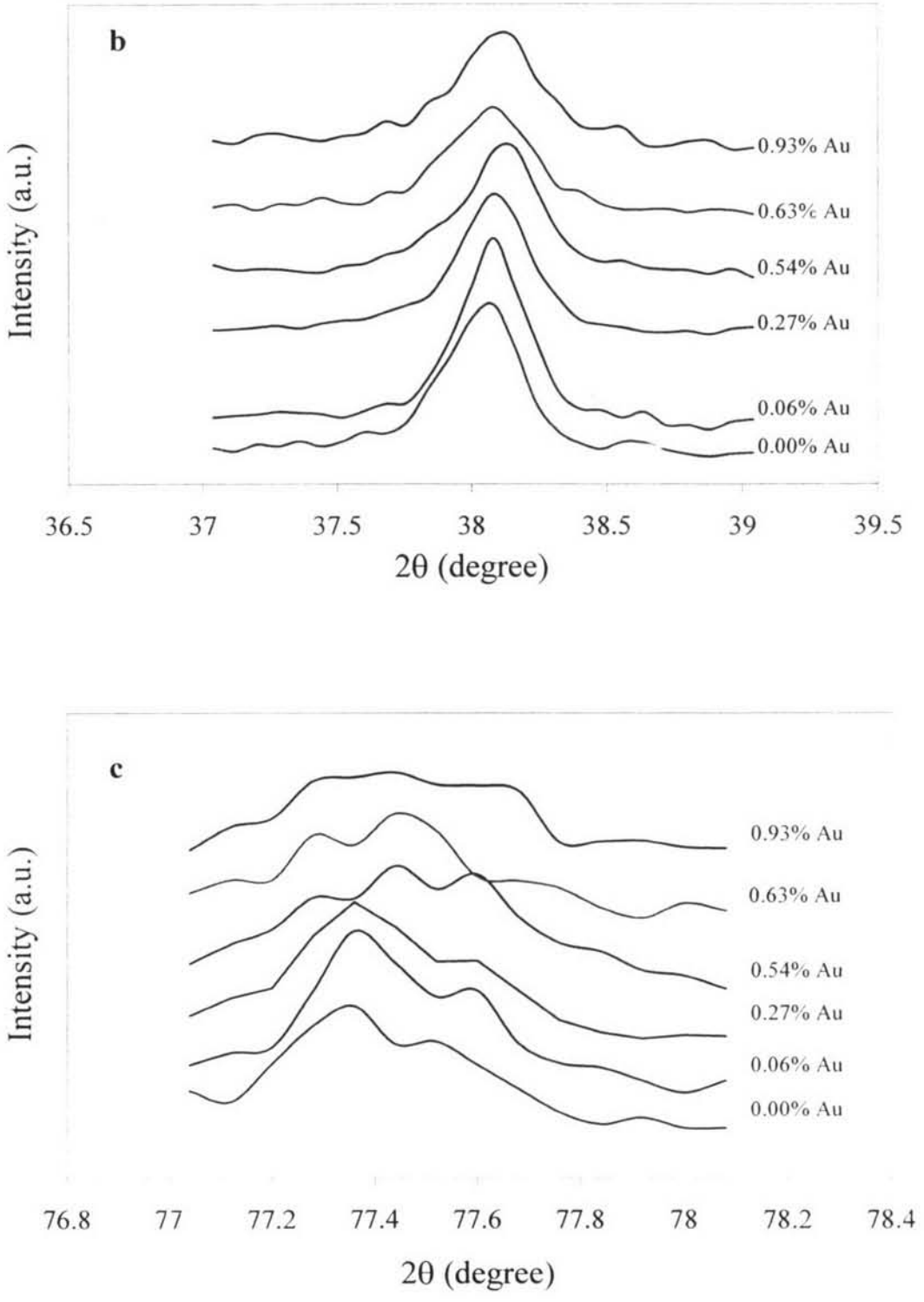

Figure 4.13 (cont'd) XRD patterns of 13.18% Ag/Al_2O_3 at various gold loadings: (b) (111) region; (c) (311) region;

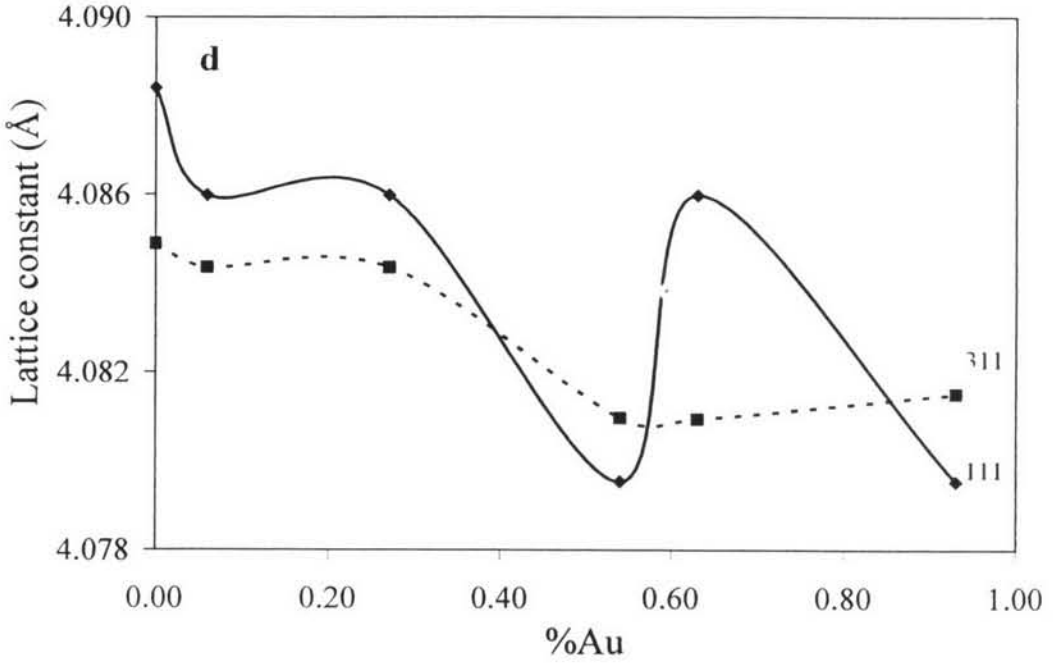

Figure 4.13 (cont'd) XRD patterns of 13.18% Ag/Al_2O_3 at various gold loadings: (d) lattice constant.

Table 4.3 Mean crystallite sizes of silver-gold catalysts for 13.18% Ag/Al_2O_3 at various gold loadings

Catalysts	Mean crystallite size, Å
0.06% Au-13.18% Ag/Al_2O_3	181
0.27% Au-13.18% Ag/Al_2O_3	186
0.54% Au-13.18% Ag/Al_2O_3	183
0.63% Au-13.18% Ag/Al_2O_3	186
0.93% Au-13.18% Ag/Al_2O_3	180

Scanning transmission electron microscopy with EDS was used to examine the size of particles and to identify the type of metal in individual particles. Figure 4.14 (a) and (b) show transmission electron micrographs of the 0.93% Au - 13.18% Ag/Al_2O_3 catalyst. Figure 4.14 (a) displays a region of the catalyst,

containing many particles with high contrast. EDS indicated that these high contrast particles contained either metallic silver or silver oxide, but no gold signal was detected. However, in other regions of the catalyst, as shown on Figure 4.14 (b), EDS detected both gold and silver within individual particles as shown in Figure 4.14 (c). Among the catalyst regions investigated, no monometallic Au particles were found. It appears that the sequential impregnation resulted in a catalyst where some of the silver particles were covered with gold. However, from X-ray diffraction it can be implied that gold and silver do not form large Au-Ag alloy particles, but gold is most likely deposited on top of Ag particles. We cannot rule out the possibility that on some particles a thin Ag-Au alloy over layer has formed.

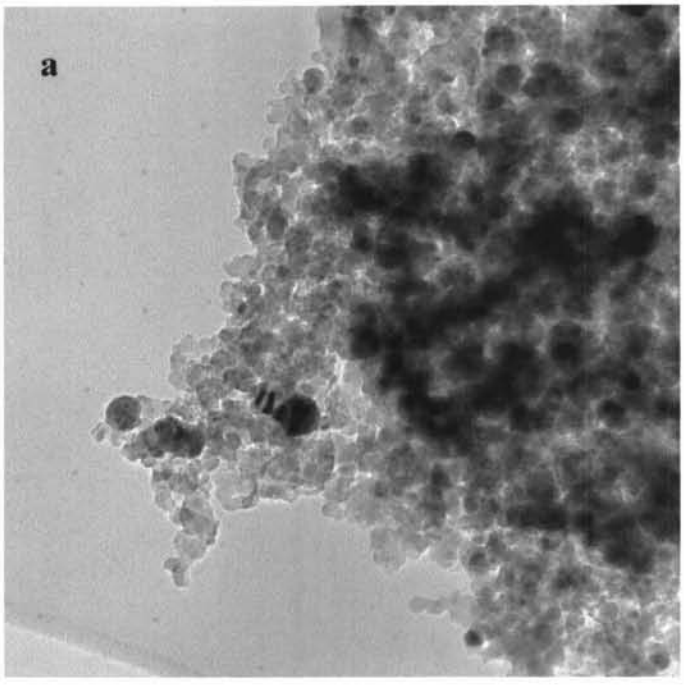

Figure 4.14 STEM micrographs of 0.93% Au-13.18% Ag/Al_2O_3: (a) aggregates of silver and silver oxide without Au;

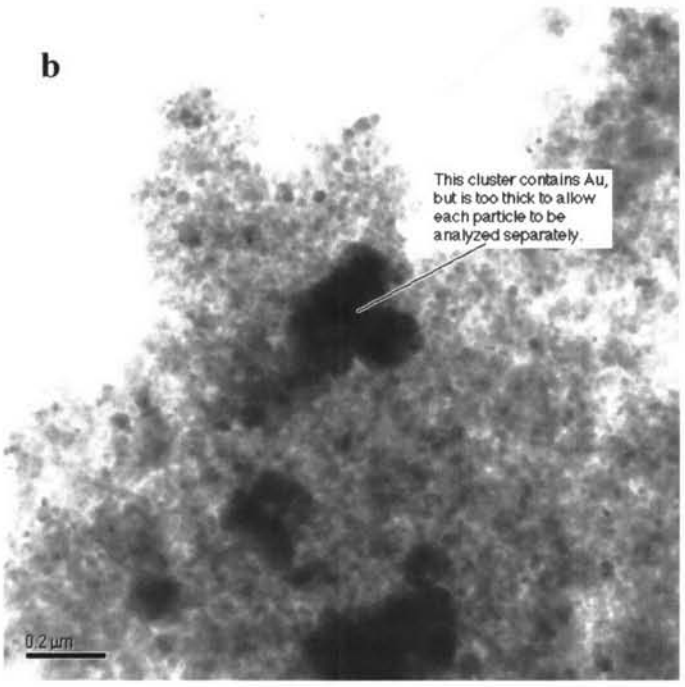

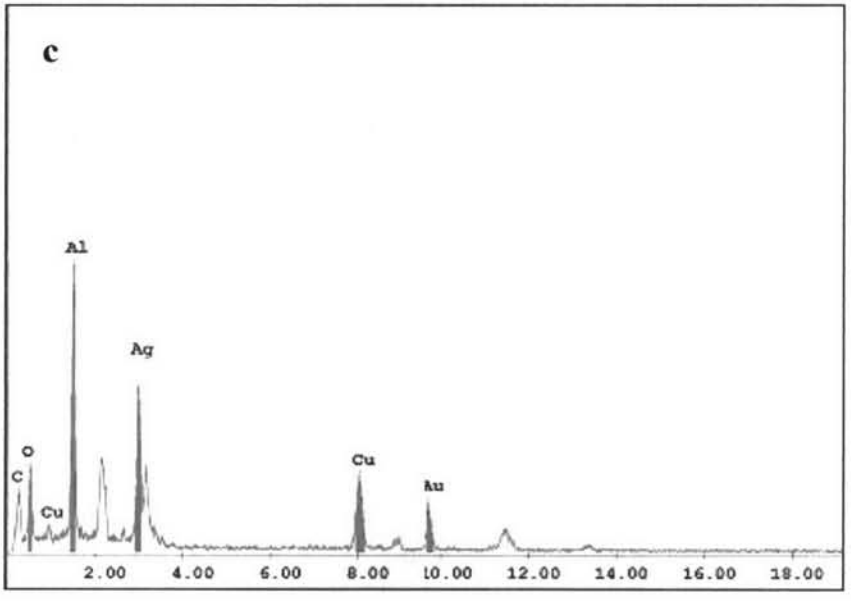

Figure 4.14 (cont'd) STEM micrographs of 0.93% Au-13.18% Ag/Al_2O_3: (b) aggregates with Au; (c) EDS profile.

4.2.2 Catalyst Activity for Epoxidation of Ethylene

Form the previous work, 13.18% Ag/Al_2O_3 loading and space velocity of 6,000 h^{-1} were identified as the optimum conditions. Therefore, the effect of gold was studied under these conditions. Gold was added in the range of 0.06, 0.27, 0.54, 0.63, and 0.93% wt, to the catalyst with optimal silver loading (13.18% Ag/Al_2O_3). An addition of gold can improve significantly ethylene oxide activity as shown in Figures 4.15-4.16. The highest ethylene oxide selectivity of 90% is obtained on the catalysts containing 0.63% Au, but the highest ethylene oxide yield is obtained on the sample with 0.54% Au at 240°C (Figure 4.17). It is interesting to note that the catalyst with the highest yield showed a significant shift of the XRD peak. The reason why adding gold gives good ethylene oxide selectivity can be explained that gold acts as a diluting agent on the silver surface and creates new single silver sites, which favor molecular oxygen adsorption (Kondarides and Verykios, 1996). This molecular oxygen reacts with ethylene into ethylene oxide according to the mechanism proposed by Campbell (1985) and in agree with the TPD results. For the blank Au/Al_2O_3, a small of desorbed O_2 was found by

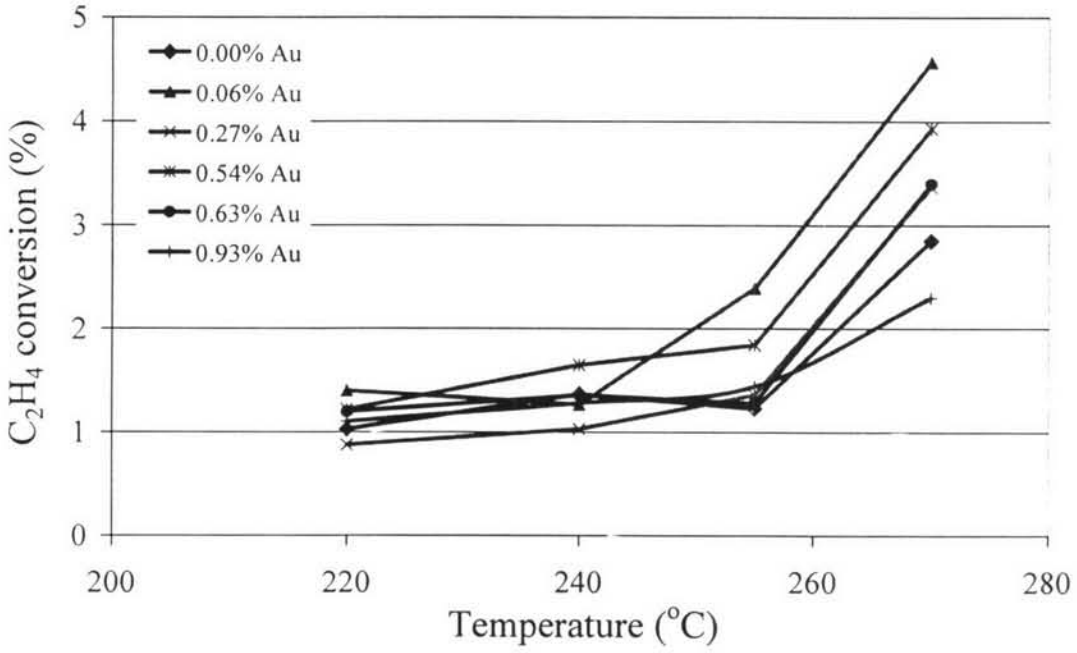

Figure 4.15 Ethylene conversion for 13.18% Ag/Al_2O_3 at various gold loadings at space velocity of 6000 h^{-1}, P = 10 psig and 6% O_2 and 6% C_2H_4 balance with He.

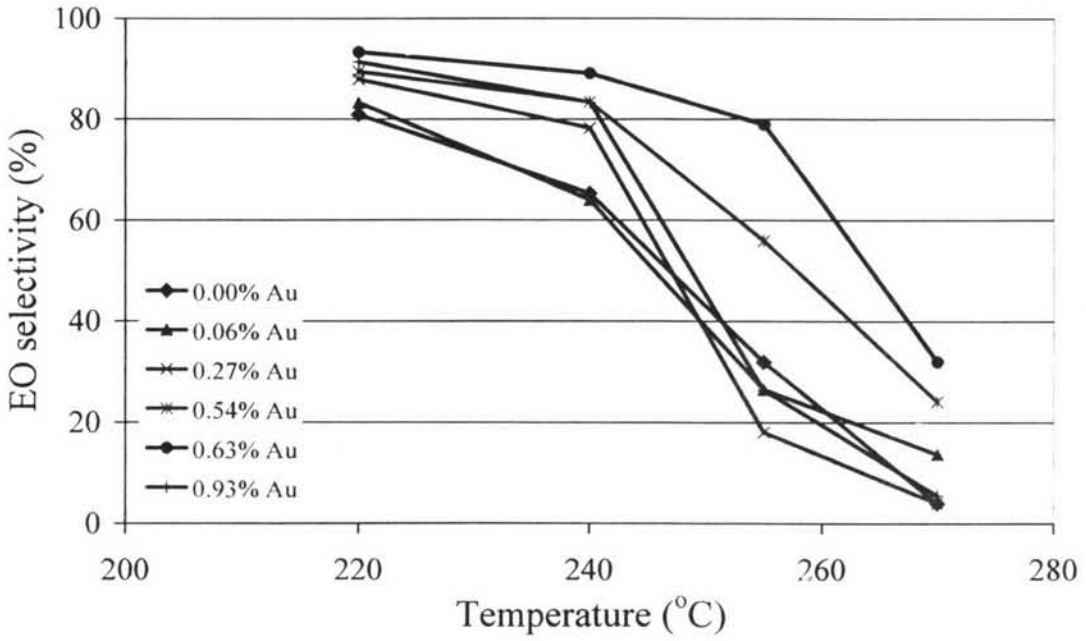

Figure 4.16 Ethylene oxide selectivity for 13.18% Ag/Al_2O_3 at various gold loadings at space velocity of 6000 h^{-1}, P = 10 psig and 6% O_2 and 6% C_2H_4 balance with He.

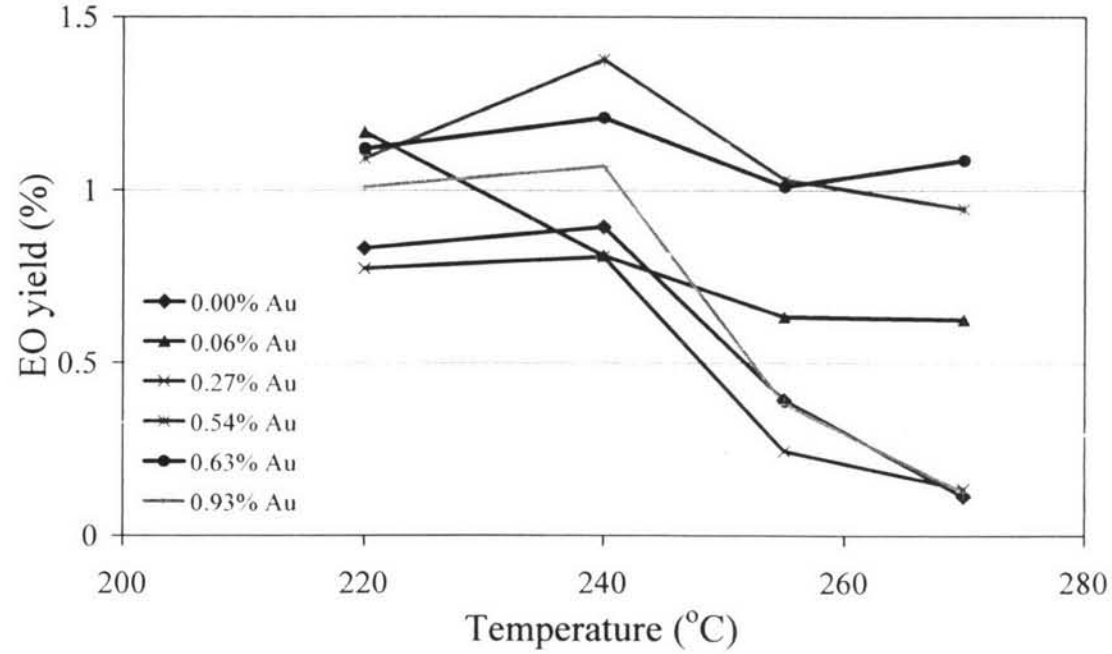

Figure 4.17 Ethylene oxide yield for 13.18% Ag/Al_2O_3 at various gold loadings at space velocity of 6000 h^{-1}, P = 10 psig and 6% O_2 and 6% C_2H_4 balance with He.

TPD, However, no enhance of ethylene oxidation was observed on this catalysts. Therefore, one can neglect the effect of residual chorine from the use of auric acid in catalyst preparation, as the promoter effect of halogen is noticeable here. It is noteworthy that adding a small amount of Au to Ag supported on amorphous Al_2O_3 improves the ethylene oxide selectivity and yield. Therefore, Au represents a promising promoter for the epoxidation reaction of ethylene.

The presence of ethylene oxide was confirmed by DRIFTS experiment over the bimetallic Au-Ag catalyst compared to the monometallic Ag catalyst as shown in the Figure 4.18. The reaction was done over the catalysts at 220°C with continuous flows of different gases and the FT-IR spectra of the bulk gas phase over the catalysts were collected after 30 min. The spectra of the effluent gas were found to have epoxy ring (800-1300 cm^{-1}) and CH-bend (1300-1600 cm^{-1}) (Skoog *et al.*, 1998). In addition, there are bands of CO_2 at 2317 and 2360 cm^{-1}. From the FT-IR results, it confirms that ethylene oxide can be produced over these

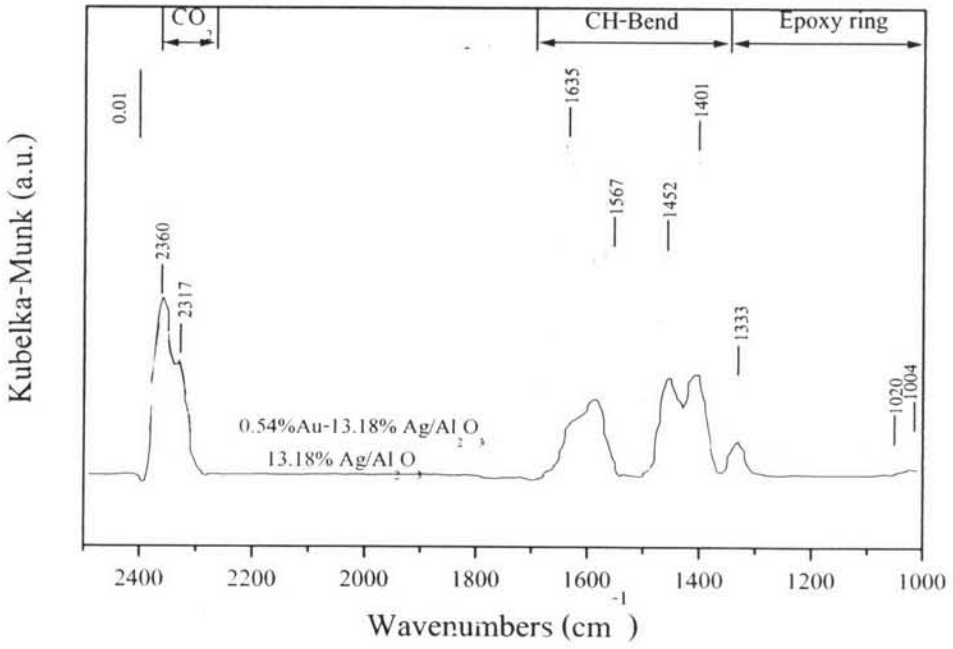

Figure 4.18 DRIFTS spectra of 0.54%Au-13.18% Ag/Al2O3 compare to 13.18% Ag/Al2O3 samples recorded after 30 min exposure of gas mixture with concentration ratio of C2H4:O2 = 2%:2%.

catalysts. Moreover, it was observed that the bimetallic Au-Ag catalyst was more active than the monometallic Ag catalyst corresponfing to the activity study results. By the way, it is noteworthy that adding a small amount of Au to Ag support on amorphous Al_2O_3 improves the ethylene oxide selectivity and yield.

4.2.3 Conclusions

Based on the STEM-EDS results, it can be concluded that the gold-silver catalysts contain an inhomogeneous distribution of gold. Some particles are metallic silver and silver oxide, while some other particles contain both silver and gold. No evidence was found for separate gold particles. The mean particle size of the bimetallic silver-gold catalysts was around 180-186 Å compared with 180-190 Å for the monometallic Ag catalyst. Impregnation of the silver catalyst with gold did not appear to change the particle size. The TPD of oxygen showed a slight shift towards lower temperature with increasing gold loading. This indicates that there must be an interaction between Ag and Au causing a weakening of the adsorption bond strength between silver and oxygen. Within the range of gold loadings investigated, the catalyst containing 0.54 %wt Au on 13.18 %wt Ag/Al_2O_3 gave the highest activity and yield of ethylene oxide. In agreement with previous suggestions in the literature, the effect of gold is attributed to a geometric effect where the silver surface is diluted, creating single silver sites that favor molecular oxygen adsorption, which react with ethylene to produce ethylene oxide.

4.3 Ethylene Epoxidation on TiO_2 Supported Au Catalysts

Studies of well-known strong metal-support interaction (SMSIs) when the support is a reducible oxide have deserved an extensive attention. The migration of oxygen from reduced support particles onto metallic particles can induce formation of a suboxide of the support, the reduction being induced by the metallic particles (Holgado *et al.*, 1998). A strong metal-support interaction effect of a group VIII noble metal and TiO_2 support is well known. Shastri *et al.* (1984) compared the behavior of gold supported on TiO_2 with other typical catalyst support materials. TiO_2 could stabilize as well as provide high dispersion of Au up to 700°C. It was suggested that this phenomenon did not appear to be due to the SMSI effect. Though a temperature of 700°C was sufficient to accomplish complete phase transformation of anatase to rutile in blank TiO_2, but no transformation occurred under identical conditions when TiO_2 was impregnated with Au. Au/TiO_2 is well known that it is good for low temperature, water-gas shift and propylene epoxidation; therefore, it should also be applicable for ethylene epoxidation.

4.3.1 Characterization Results

Oxygen TPD experiments of Au/TiO_2 catalysts prepared by different methods were carried out with and without cooling step as described in previous works (chapter 4.2). As be seen from Figures 4.19-4.20, desorption profiles of oxygen with and without cooling step have the similar trend. Interestingly for three prepared catalysts and blank TiO_2, large desorption peaks were observed at around 400°C (with cooling step) and 460°C (without cooling step). These broad desorption peaks are assigned to desorbing of oxygen from TiO_2 support due to the removal of lattice oxygen from subsurface regions causing the creation of oxygen vacancies (Walton *et al.*, 1997). Typically, molecular oxygen desorbs from oxide surfaces between 27 to 127°C (Bielanski and Haber, 1991). As expected, 0.96% Au/TiO_2 sol gel gave the largest amount of desorption peak. The reason is that Au particle size of this catalyst is the smallest and better distribution on the support as compared to those with the other two preparation methods according to the TEM results. Therefore, there are more active sites that O_2 can be adsorbed and the interaction

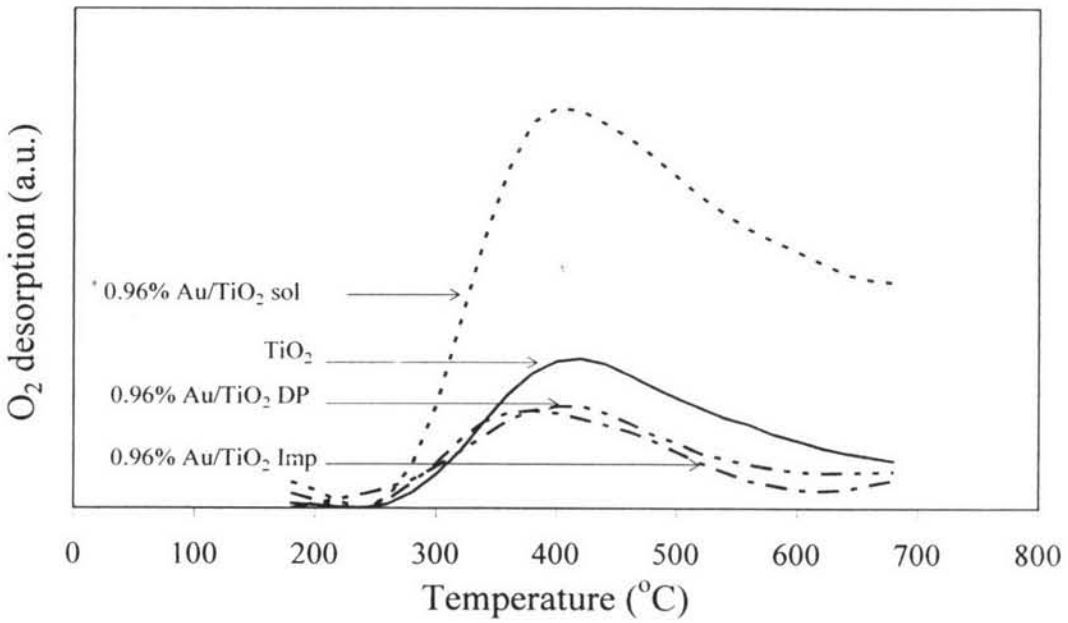

Figure 4.19 TPD profiles of O_2 with cooling step on Au/TiO_2 catalysts prepared with different methods.

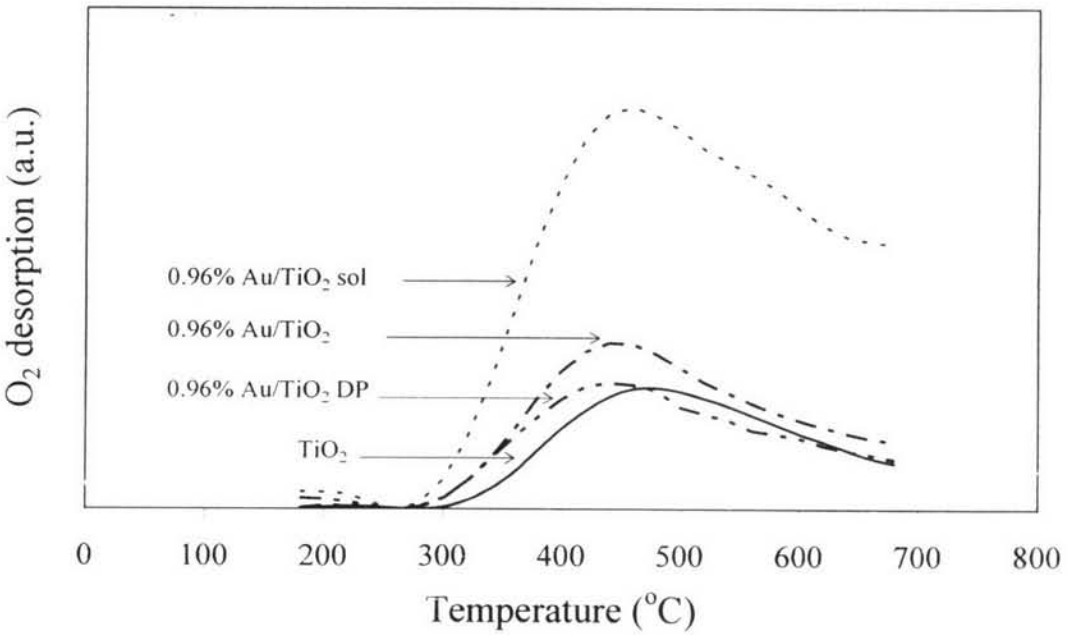

Figure 4.20 TPD profiles of O_2 without cooling step on Au/TiO_2 catalysts prepared with different methods.

between Au and O_2 is weakened and easy to desorb (Hayashi *et al.*, 1998). In addition, it is noticeable that an addition of gold on TiO_2 support affected to shift oxygen desorption peaks to lower temperature for all preparation methods as compared to the blank TiO_2. It can be explained in term of electronic effect that there are electrons transfer between gold atom and TiO_2 support while adsorbed oxygen also requires transfer of electrons between TiO_2 support and oxygen. Therefore, it is expected that the electron deficiency due to the neighbor interaction between gold atom results in weakening of Ti-O bond.

Figure 4.21 shows the oxygen desorption difference with and without cooling steps of different Au/TiO_2 catalysts. It has been known that the oxygen desorption in the range of 227-527°C may be ascribed to one or combination of following effects; spill over oxygen (Bielanski and Haber, 1991), surface and sub-surface lattice oxygen (Komuro, 1975) and oxygen from Au sites (Walton *et al.*, 1998a). Therefore, the highest desorption peaks at around 300-400°C are assigned to oxygen that adsorbs on the surface or subsurface on TiO_2. As can be seen from Figure 4.21, it is noticeable that for each catalyst, there is another peak of oxygen desorption below 200°C due to the molecular oxygen on Au active site (Schwank, 1983). Furthermore, oxygen desorption from the TiO_2 support is confirmed using helium as an exposure gas instead of O_2 as shown in Figure 4.22. The result insists that oxygen desorbs out from the TiO_2 support at higher temperatures in the range of 300-600°C. It is observed from the TPD results that the oxygen desorption peak with helium exposure gives a little bit higher amount of desorbed oxygen than that with O_2 exposure. It can be explained that TiO_2 is a nonstoichiometric material. There are two main defects for titania known as oxygen vacancies and interstitial Ti^{3+} ions. When the catalyst is exposed with O_2, the titania support will anneal oxygen vacancies with oxygen adsorption into the surface and subsurface region of the lattice (Komuro, 1975 and Walton *et al.*, 1998b). This result in higher stability of the lattice causing desorption of O_2 at higher temperatures than exposure with helium. When the catalyst is exposed with helium at higher temperatures, the titania will produce the defect of lattice causing unstable support. Therefore, oxygen on the surface or subsurface desorbs out more easily.

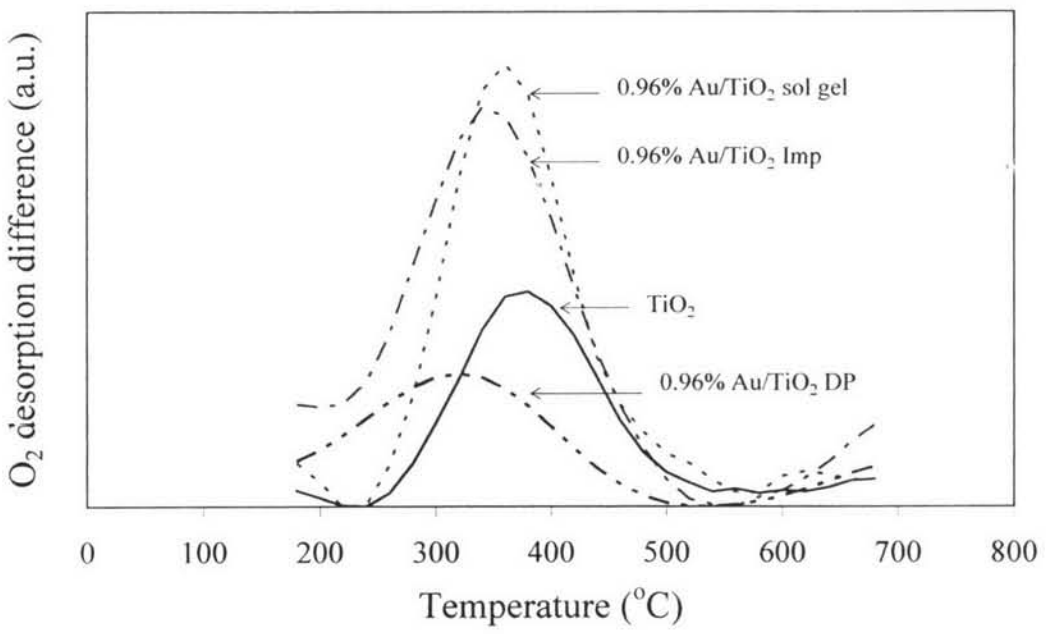

Figure 4.21 O_2 desorption difference between TPD runs with and without cooling step of different Au/TiO_2 catalysts.

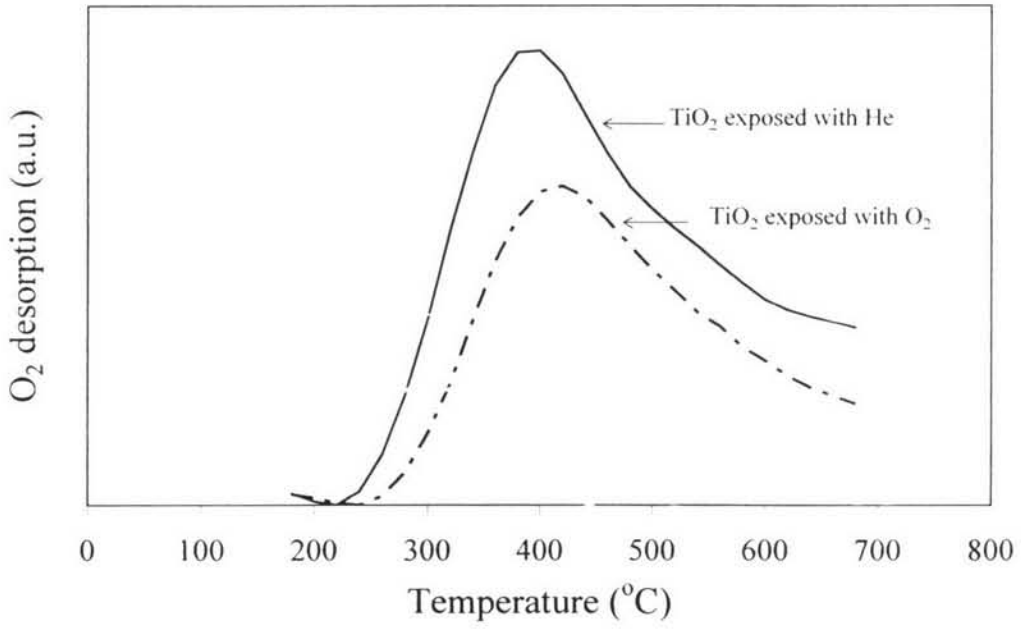

Figure 4.22 Comparison of O_2 TPD between TiO_2 (P25) exposed to He and O_2.

The XRD results of Au on TiO_2 catalyst prepared with different techniques are compared with pure TiO_2 and shown in Figure 4.23. The results show that 0.96% Au/TiO_2 with impregnation (Imp) and 1.28% Au/TiO_2 deposition-precipitation (DP), prepared by TiO_2 P25 from Degussa, are composed of both anatase (A) and rutile (R) phase because this commercial TiO_2 support is composed of these two phases. On the other hand, 0.96% Au/TiO_2 (sol gel) shows only anatase phase. All three catalysts have similar BET surface areas around 60 m^2/g.

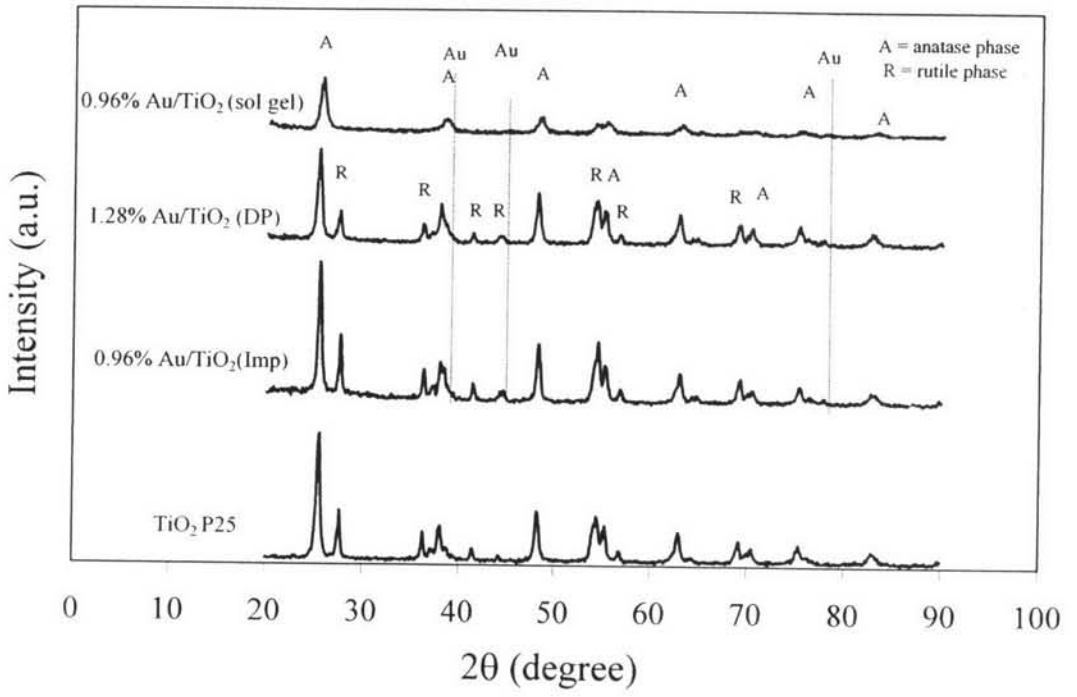

Figure 4.23 XRD patterns of Au/TiO_2 catalysts prepared with three different methods compared to XRD patterns of commercial TiO_2.

As expected, the gold peaks are not clearly discernible from these XRD patterns, however very small peaks at 38.27°, 44.65° and 77.58° could be seen. The gold catalysts prepared have nanosize gold particles which are undetectable by XRD equipment. However, the average crystallite sizes of Au/TiO_2 catalyst prepared by impregnation, deposition-precipitation and sol gel were 23, 19 and 37 nm, respectively, calculated using the Scherer equation.

The SEM morphology of 0.96% Au/TiO_2 (Imp)(Figure 4.24 (a)) and 1.28% Au/TiO_2 (DP) (Figure 4.24 (b)) has rough surface cluster while 0.96%

Au/TiO_2 (sol gel) has distinctly smooth clusters (Figure 4.24 (c)). The reason is that Au and Ti are formed as solid solution for sol gel technique while the others are deposition of gold on the surface of the support.

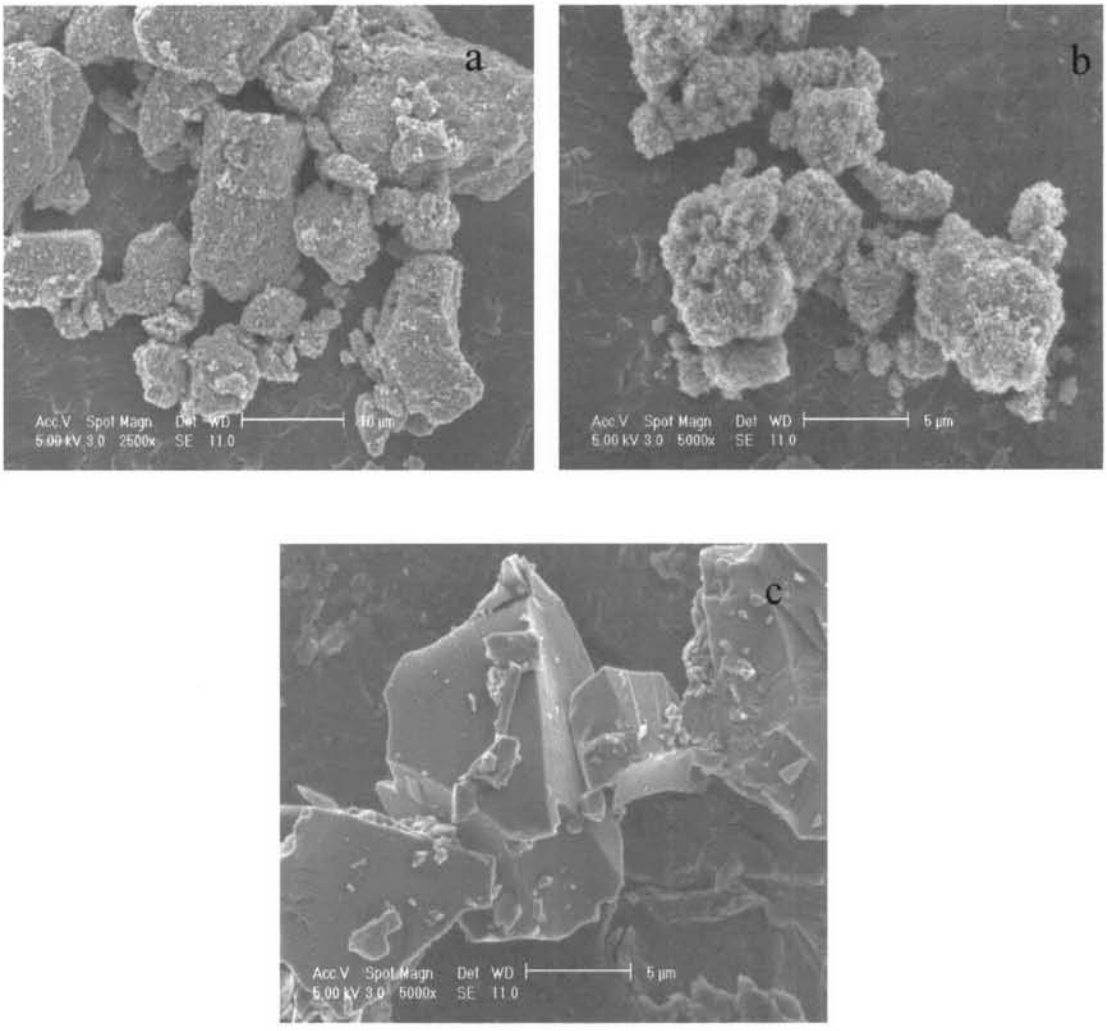

Figure 4.24 SEM surface morphology of gold catalysts prepared by different methods: (a) impregnation; (b) deposition-precipitation; (c) sol gel.

The TEM micrographs shown in Figures 4.25-4.27 reveal the presence of the gold particles as dark spots appear in the catalyst clusters. The existence of gold particles on TiO_2 support was verified by using EDS focusing on the regions containing highly contrast spots under transmission electron microscope. For 0.96% Au/TiO_2 (Imp), the gold particles were seen as highly contrast spots both on and inside the support and average particle size of is around 3.2 ± 0.7 nm (Figure 4.25). In addition, 1.28% Au/TiO_2 (DP) catalyst apparently had a smaller Au particle

size in the range of 2.5 ± 0.6 nm (Figure 4.26). Figure 4.27 presents the TEM micrograph of 0.96% Au/TiO_2 (sol gel). It can be seen that the sol gel method provides better distribution of Au than the other two methods and Au particle size is much smaller in the range of 1.2 ± 0.3 nm. Therefore, all Au on TiO_2 catalysts prepared by three different methods have nanoparticle sizes in the sequence of particle size from sol gel <deposition-precipitation< impregnation.

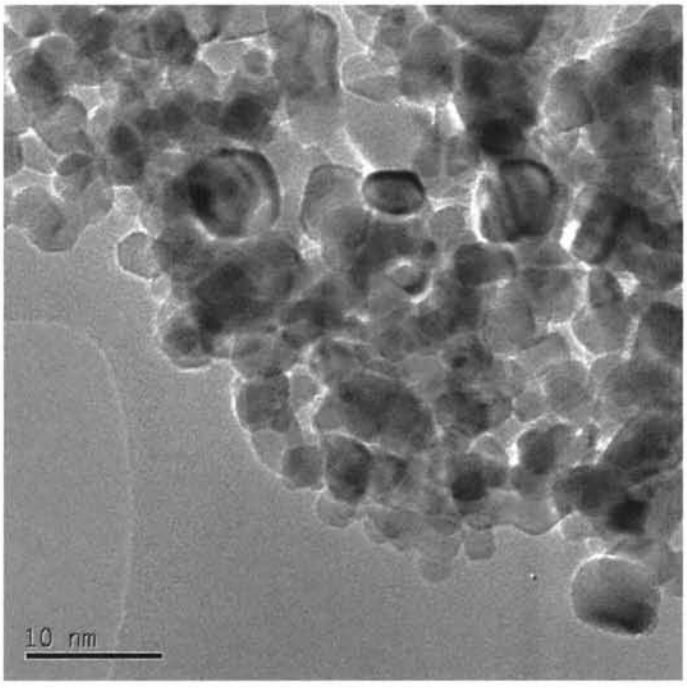

Figure 4.25 Gold particles (dark spots) on the TiO_2 surface for 0.96% Au/TiO_2 catalyst prepared by impregnation method.

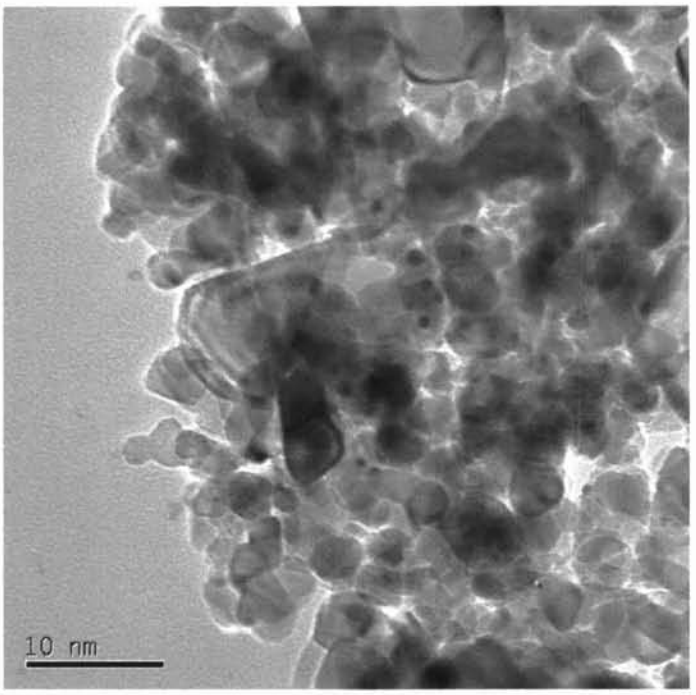

Figure 4.26 Gold particles (dark spots) on the TiO_2 surface for 1.28% Au/TiO_2 catalyst prepared by deposition-precipitation method.

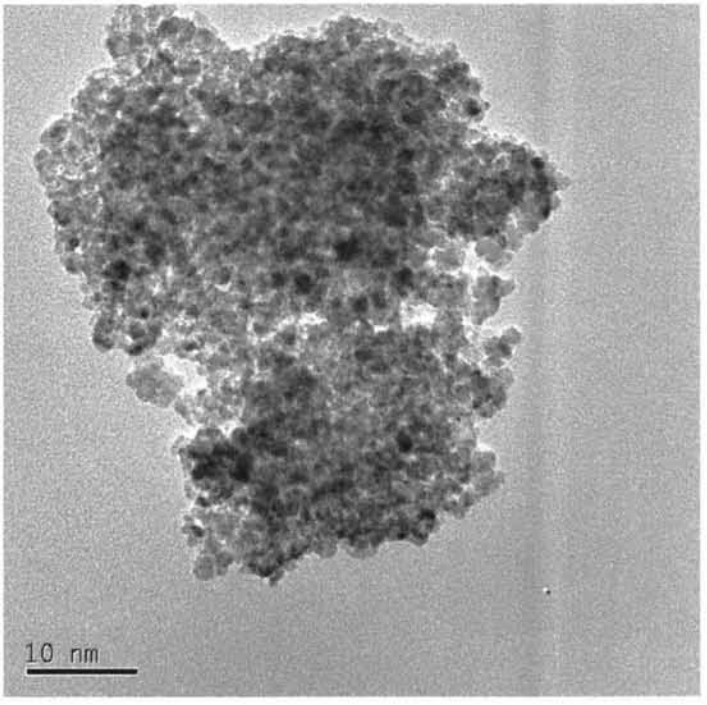

Figure 4.27 Gold particles (dark spots) on the TiO_2 surface for 0.96% Au/TiO_2 catalyst prepared by sol gel method.

4.3.2 Catalyst Activity of Ethylene Epoxidation

Figures 4. 28 and 4.29 illustrate the effect of temperature on the ethylene epoxidation activity of Au/TiO_2 catalysts prepared by three different methods. For all studied catalysts, the ethylene conversion increased with increasing reaction temperature, while the selectivity of ethylene oxide decreased with increasing reaction temperature as a result that there are two competitive reactions between the partial oxidation and deep oxidation. For the deep oxidation reaction, both ethylene and ethylene oxide react with oxygen derived from the support to produce carbon dioxide and water. As be known, a higher temperature leads to a higher rate of deep oxidation reaction resulting in lowering ethylene oxide selectivity. Furthermore, 0.96% Au on TiO_2 with impregnation gave both the highest ethylene oxide selectivity and yield as compared to other two catalysts prepared by deposition-precipitation and sol gel methods (Figures 4.28-4.30). From the results of the present study, it is clearly seen that there is a good correlation between the particle size of gold and activity of ethylene epoxidation reaction. It has been reported that oxygen species are formed at the perimeter interface between the gold particles and the TiO_2 support when the particle size is greater than 2 nm (Hayashi *et al.,* 1998). These oxygen species located at the perimeter interface are mostly molecular oxygen (MacDonald and Hayes, 1970 and Schwank, 1983 and Haruta and Date, 2001) which is responsible for reacting directly with ethylene in the gas phase to produce ethylene oxide. The results showed that the maximum yield of ethylene oxide was found to be about 1% at 255°C for 0.96% Au/TiO_2 (Imp) and around 0.8% for 1.28% Au/TiO_2 (DP). On the other hand, 0.96% Au/ TiO_2 (sol gel) gave the maximum ethylene oxide yield of 0.6% at 240°C. As be mentioned earlier, the TPD results confirm that the interaction between oxygen molecule and Au is weakened leading to the promotion on ethylene oxide. Interestingly, the impregnation method could provide the largest gold particle size of around 3 nm and this catalyst also gave the highest yield of ethylene oxide. The results indicate that the ethylene oxide selectivity is governed by the particle size of gold which a larger gold particle size will weaken the interaction between the gold particles and the TiO_2 support to promote molecular oxygen adsorption at the perimeter interface enhancing ethylene oxide formation. However, more experimental work will be required to verify these

mechanistic ideas. The way to prove this mechanism is by using isotopic oxygen, O^{18} and O^{16}, to clarify the adsorbed location and adsorbed oxygen species on catalysts.

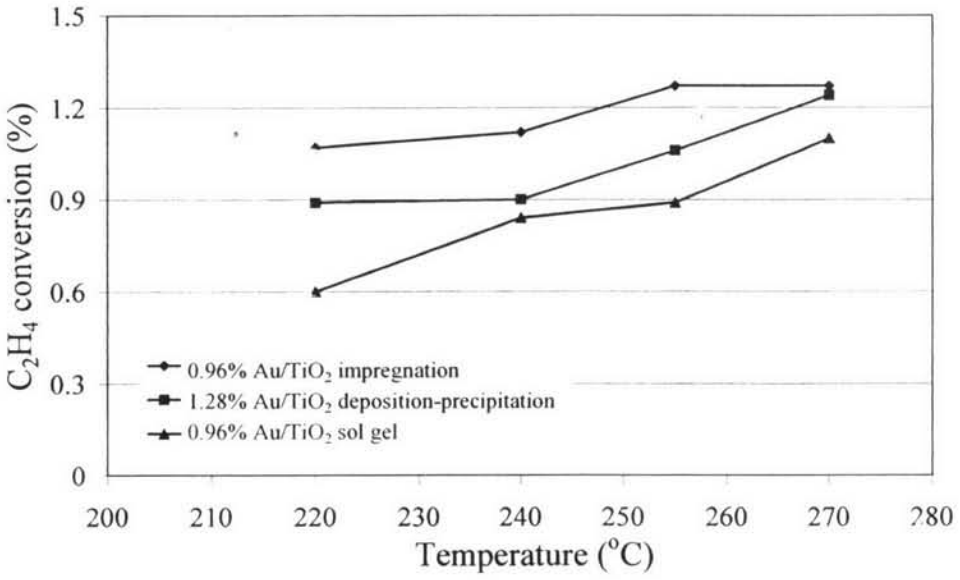

Figure 4.28 Ethylene conversion for different catalyst preparations at space velocity of 6,000 h^{-1}, P = 10 psig and 6% O_2 and 6% C_2H_4 balance with He.

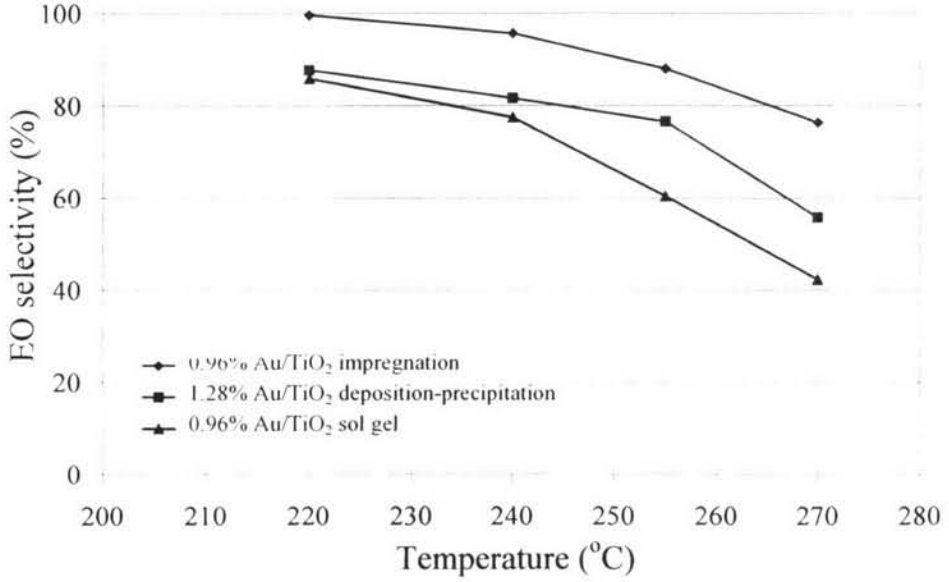

Figure 4.29 Ethylene oxide selectivity for different catalyst preparations at space velocity of 6,000 h^{-1}, P = 10 psig and 6% O_2 and 6% C_2H_4 balance with He.

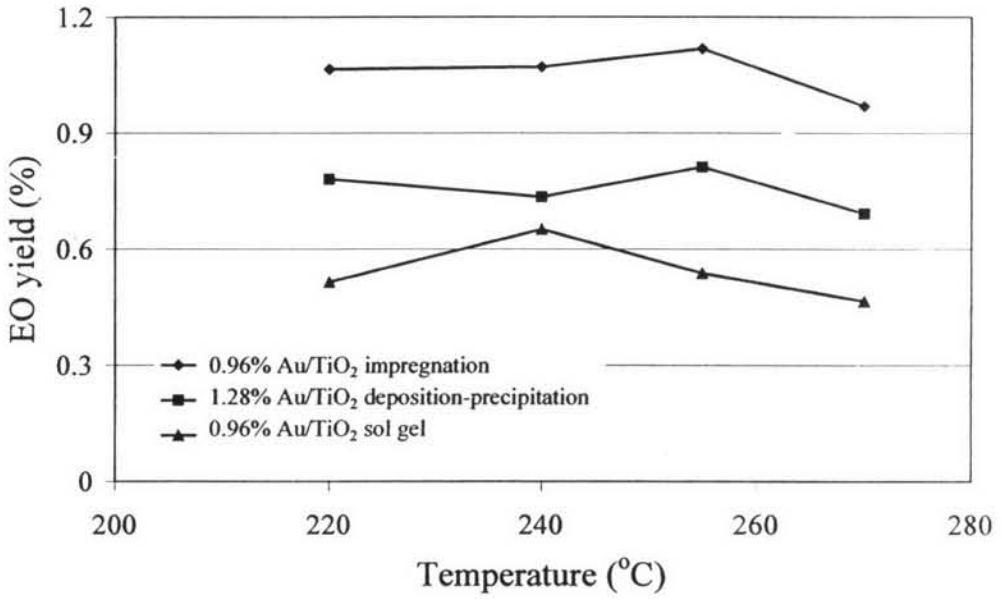

Figure 4.30 Ethylene oxide yield for different catalyst preparations at space velocity of 6,000 h^{-1}, P = 10 psig and 6% O_2 and 6% C_2H_4 balance with He.

The presence of ethylene oxide was conformed by the subsequence reaction detected with mass spectrometry (as shown in Appendix A, Figure A.2). With this technique, the result showed trends of ethylene oxide present, but it was not absolutely clear. Therefore, DRIFTS reaction was employed to prove ethylene oxide produced over the catalyst. FT-IR results of the catalytic oxidation of ethylene are shown in the Figures 4.31-4.33, the reaction was carried out at 220°C in the gas phase and the FT-IR spectrum was collected every interval time of 5 min until 30 min of reaction. A blank experiment was also conducted using a pure TiO_2 support and it was found no reaction occurring in the studied conditions. These bands are compared with library's information provided that spectra were attributed to CH-bend (1300-1700 cm^{-1}), epoxy ring (800-1300 cm^{-1}) and CO_2 functional groups (2300-2400 cm^{-1}) (Skoog *et al.*, 1998). For 0.96% Au/TiO_2 (Imp), the spectrum of pure ethylene exposed for 30 min over Au/TiO_2 catalyst used as a blank as shown in Figure 4.31, curve a. The spectra (at 1065, 1330, 1445 and 1717 cm^{-1}) increased with increasing exposure time (Figure 4.31, curves b-g) compared with the curve of pure ethylene (Figure 4.31, curve a). Figure 4.32 shows that for 1.28% Au/TiO_2 (DP) the intensity of bands (1015, 1347, 1445 and 1534 cm^{-1}) increased progressively with

time as well. Similarly, the same behavior occurs for 0.96% Au/TiO_2 (sol gel) (1067, 1342, 1447 and 1530 cm^{-1}) as shown in Figure 4.33, curves a-f. It can be stated that DRIFTS results confirm the formation of ethylene oxide over studied catalyst under this conditions. Moreover, as compared to Figures 4.31-4.33 for DRIFTS spectra of ethylene epoxidation over each catalyst, 1.28% Au/TiO_2 (DP) is the most active catalyst for ethylene oxide production. Incidentally, there were spectra bands for CO_2 at 2330 and 2360 cm^{-1} observed for each catalyst to pronounce that there is combustion reaction that competed with partial oxidation on this condition.

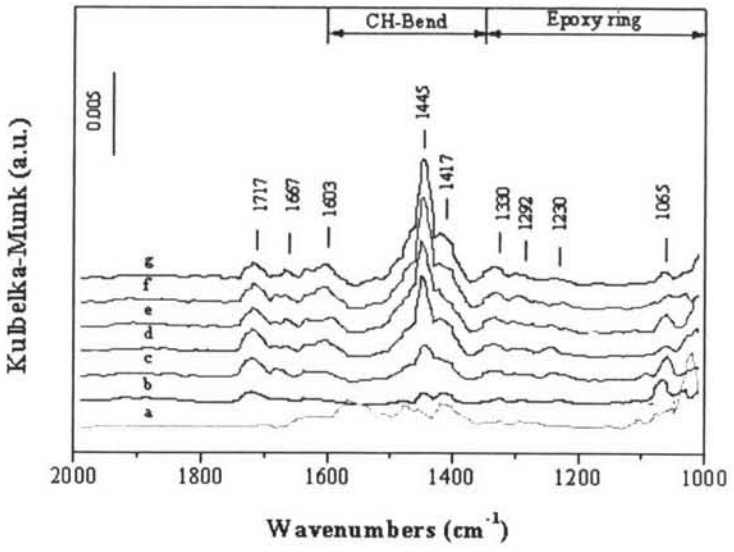

Figure 4.31 DRIFTS spectra over 0.96% Au/TiO_2 (Imp) of (a) pure ethylene at 30 min exposure time compared with 2% ethylene and 2% oxygen at different exposure times: (b) 1 min; (c) 5 min; (d) 15 min; (e) 20 min; (f) 25 min; (g) 30 min.

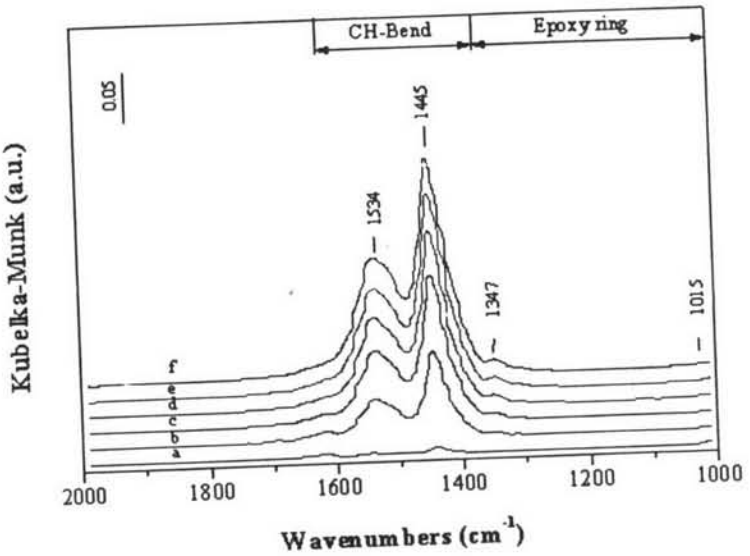

Figure 4.32 DRIFTS spectra of ethylene oxidation over 1.28% Au/TiO_2 (DP) after exposed 2% ethylene and 2% oxygen at different exposure times: (a) 1 min; (b) 10 min; (c) 15 min; (d) 20 min; (e) 25 min; (f) 30 min.

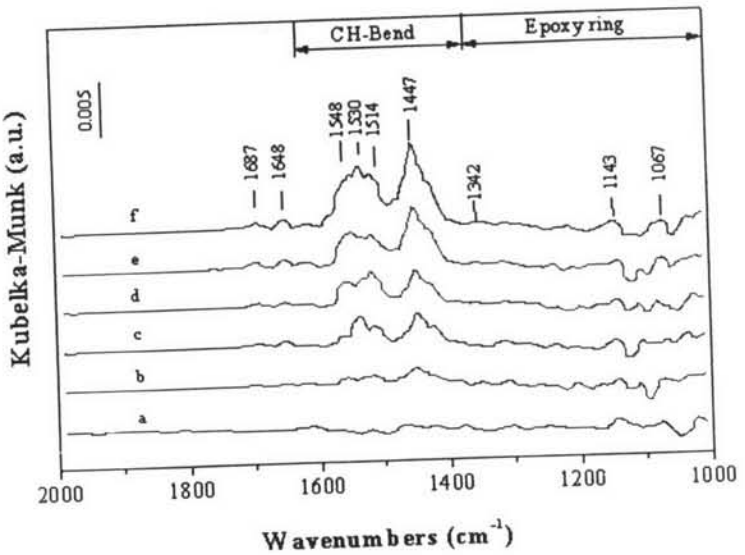

Figure 4.33 DRIFTS spectra of ethylene oxidation over 0.96% Au/TiO_2 (sol gel) after exposed 2% ethylene and 2% oxygen at different exposure times: (a) 1 min; (b) 10 min; (c) 15 min; (d) 20 min; (e) 25 min; (f) 30 min.

4.3.3 Conclusions

Au/TiO_2 is used as catalyst not only for CO oxidation, but also for epoxidation as well. This gold on TiO_2 was previously used for propylene epoxidation and found that the particle size had a significant effect on the epoxidation activity. Based on the results of present studies, it suggests that the reaction of ethylene epoxidation depends on the size of gold which is governed by a catalyst preparation method. The optimum size of gold particles was approximately 3 nm for the epoxidation reaction of ethylene. If the particle size was less than 2 nm, the reaction was difficult to occur that why the ethylene oxide yield of Au/TiO_2 (sol gel) was found to be low (0.6%). Nevertheless, these gold catalysts still give the lower activity comparing to $Au\text{-}Ag/Al_2O_3$ catalysts of the previous study (Roatluechai *et al.*, 2001).

4.4 Ethylene Epoxidation on CeO_2 Supported Au Catalysts

Ceria has an important role in most commercial catalytic processes in terms of economic relevance and tonnage: three-way catalysis (TWC) and fluid catalytic cracking (FCC). It is because ceria can stabilize supports and keep high surface area, and prevent the sintering of precious metals. Ceria is commonly used for the CO oxidation and water-gas shift reaction, resulted from its unique property as oxygen reservoir (Kaspar *et al.*, 1999 and Imamura *et al.*, 2000). In this research, gold catalysts on ceria support obtained from different preparation methods were studied for the selective oxidation of ethylene.

4.4.1 Characterization Results

TPD experiments were carried out with and without a cooling step as described in the previous study of Au as a promoter on Ag/Al_2O_3 catalysts (Roatluechai *et al.*, 2002). The TPD of oxygen for all Au/CeO_2 sol gel catalysts and pure CeO_2 sol gel with and without a cooling step are shown comparatively in Figures 4.34-4.35, respectively. From the TPD results with a cooling step, as can be seen in Figure 4.34, the maximum oxygen desorption temperatures of all Au catalysts and single-step sol gel CeO_2 were the same (475°C) and slightly higher than that of the sol gel CeO_2 (at 460°C). The results imply that the major oxygen desorption comes from the CeO_2 support. The addition of Au shows insignificantly the effect on the TPD of oxygen on CeO2 support. The similar results were also obtained for the TPD of oxygen without a cooling step. Interestingly, the TPD result of 0.88% Au/commercial CeO_2 (low surface area) showed two dominant peaks at 200°C and 450°C for with a cooling step while 300°C and 650°C for without a cooling step. The desorption peaks around 200-300°C may be ascribed to the oxygen desorbed from both Au active sites and CeO_2 support. The oxygen desorption peak beyond 300°C is believed to derive from only the CeO_2 support. In comparisons all TPD results, the amount of adsorbed O_2 on Au/commercial CeO_2 (low surface area) was much lower than those on pure sol gel CeO_2 and Au/ sol gel CeO_2 catalysts. From the TPD results without a cooing step for any given catalyst (Figure 4.35), the

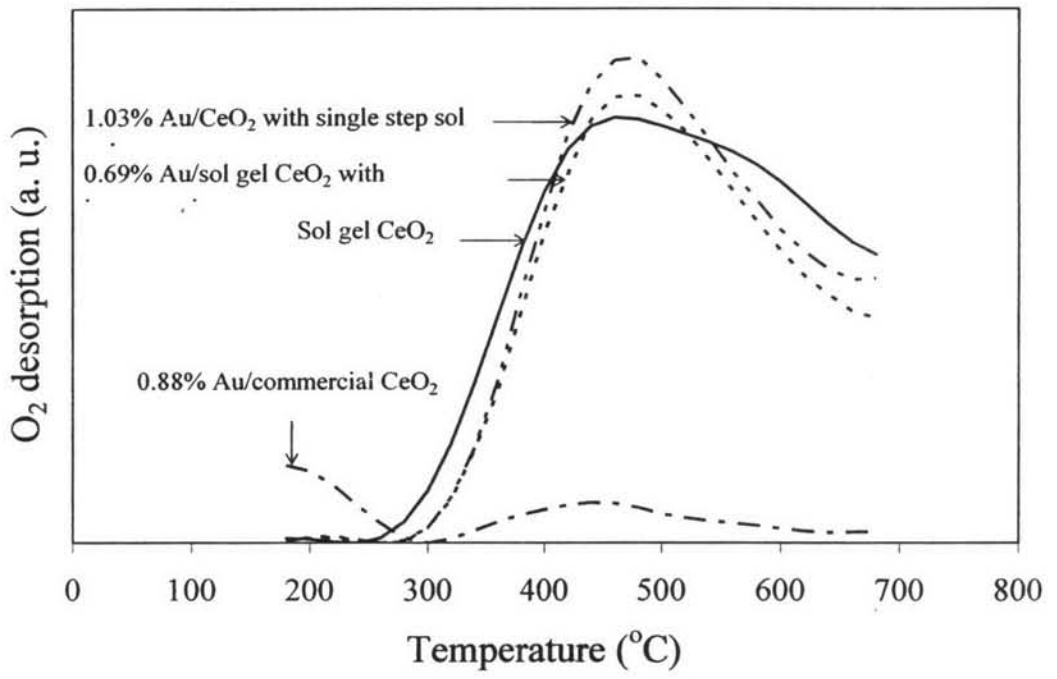

Figure 4.34 TPD profiles of O_2 with a cooling step on different Au/CeO_2 samples.

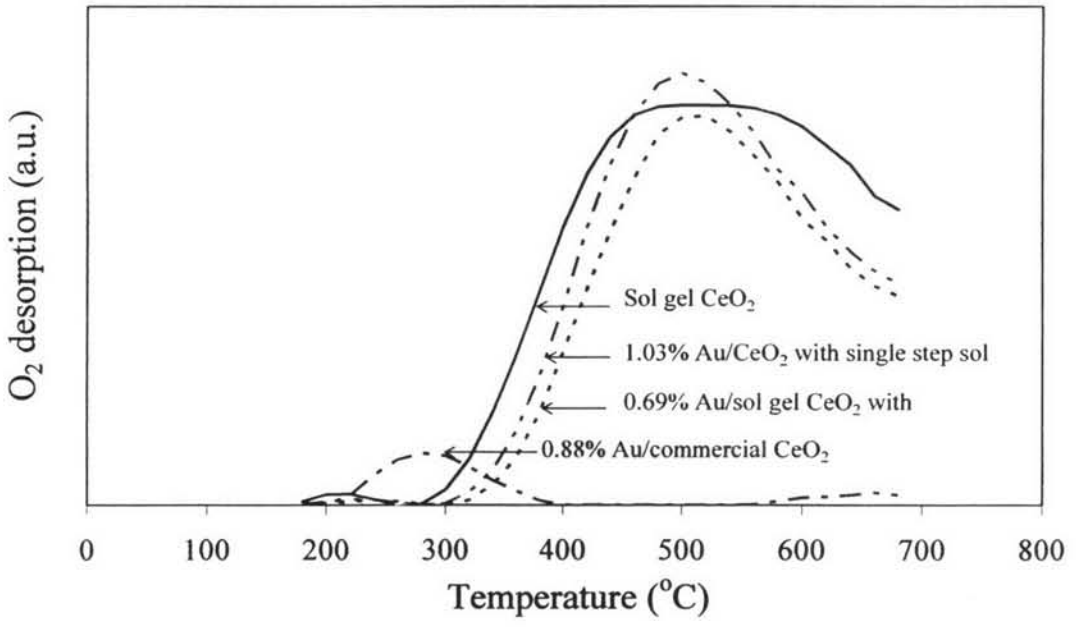

Figure 4.35 TPD profiles of O_2 without a cooling step on different Au/CeO_2 samples.

maximum oxygen desorption temperature was about 20°C higher than that with a cooling step. The results showed that the presence of Au did not show a significant effect on the maximum oxygen desorption temperature of CeO_2 which does not agree with literature. It can be explained that the Au loadings used in the present study were relatively low as compared to those of previous works. It was reported that the surface oxygen of ceria was substantially weakened in the presence of gold nanoparticle (Flytzani-Stephanopoulos, 2001 and Qi Fu *et al.*, 2001). These phenomenon was confirmed by the TPR results that the effect of gold loading depended strongly on the preparation, calcinations temperature (Flytzani-Stephanopoulos, 2001). However, very small peaks of oxygen desorption at around 200°C were observed for all catalyst samples. In order to elucidate these low temperature oxygen desorption peaks, the difference of the oxygen TPD with and without a cooling step of each catalyst sample is plotted against temperature as shown in Figure 4.36. The oxygen desorption peaks at around 200°C for all three samples are resulted from oxygen species adsorbing on the Au active sites (Schwank, 1983) and the oxygen vacancies in the CeO_2 support when being cooled down to room temperature. The desorption peaks in the range of 350-400°C are believed to derive from the adsorbed oxygen either on the support surface

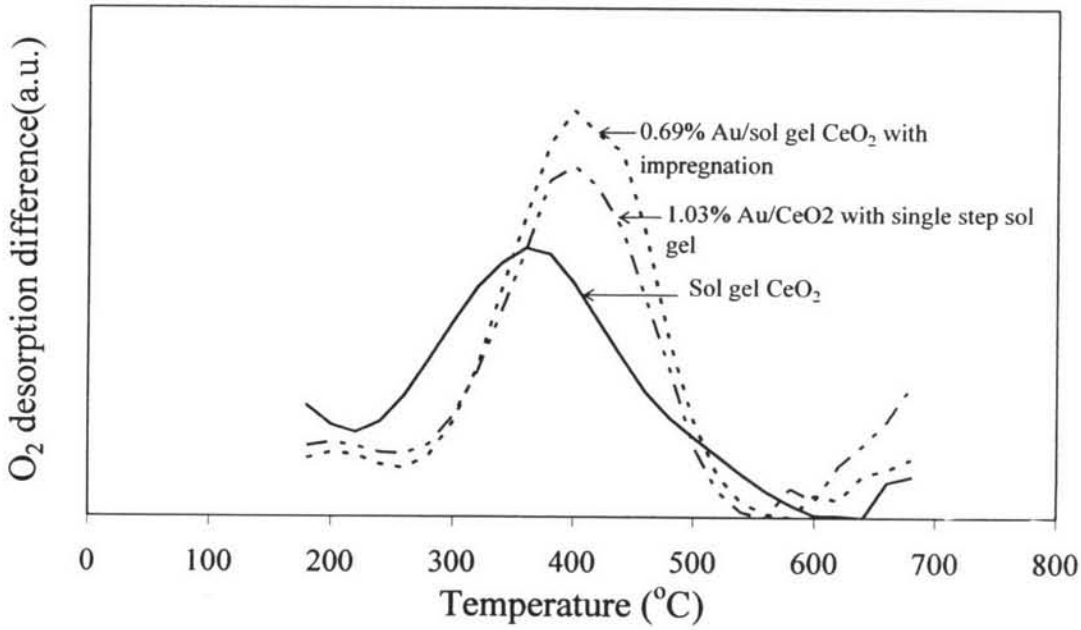

Figure 4.36 Desorption difference of TPD of oxygen with and without a cooling step over different Au/CeO_2 samples.

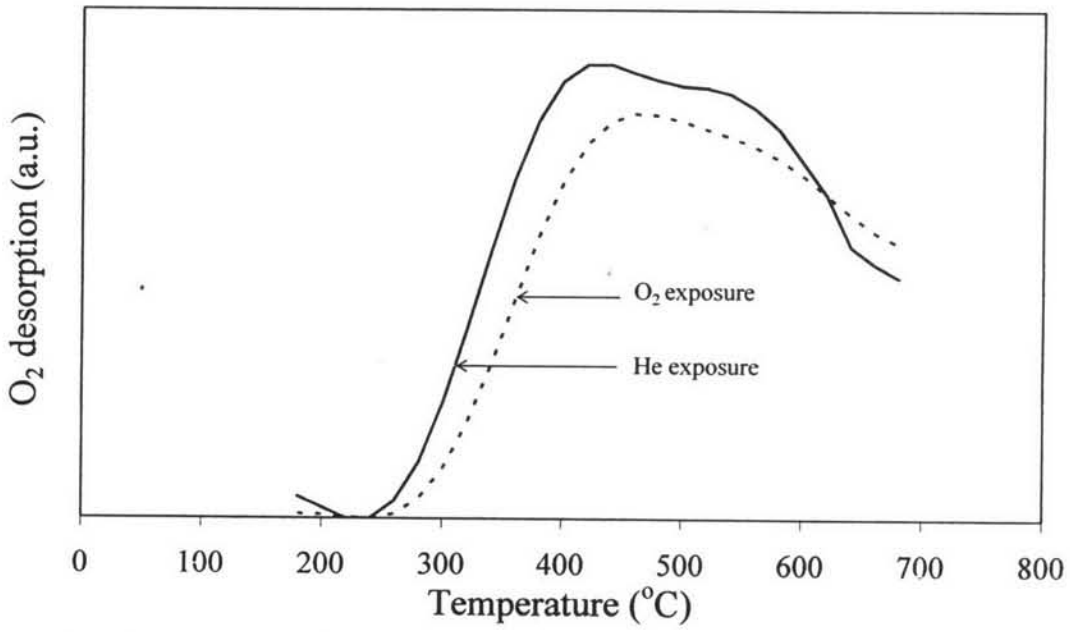

Figure 4.37 Comparison of TPD between CeO_2 sol gel exposed to He and O_2.

or from the bulk CeO_2 support not from the u surface. The oxygen desorption above 550°C comes from the bulk oxygen of the CeO_2 support. In order to verify these explanations, helium was used as an exposure gas instead of O_2 in the pretreatment step of the TPD experiment. As can be seen from Figure 4.37, it implies that the desorbed oxygen comes from the surface of CeO_2 at low temperatures (200°C) and the bulk CeO_2 support at high temperatures (400-600°C). A next question is why the TPD of oxygen with helium exposure was higher than that with O_2 exposure. The difference is believed to be due to the nonstoichiometric property of CeO_2. CeO_2 can exist in several oxidation states, typically Ce^{3+} and Ce^{4+} and the oxygen diffusion from nonstoichiometric fluorite type oxides is easier than oxygen diffusion in the stoichiometric oxides. Thus, the TPD when exposed to helium exhibits lower oxygen desorption temperature and higher oxygen desorption than those with O_2 (Sørensen, 1981).

The XRD patterns of gold on CeO_2 support are compared to that of pure CeO_2 prepared with different methods as shown in Figure 4.38. The XRD results showed that the commercial CeO_2 (low surface area) is more crystalline methods compared to that of the pure CeO_2 support. sol gel CeO_2. As expected,

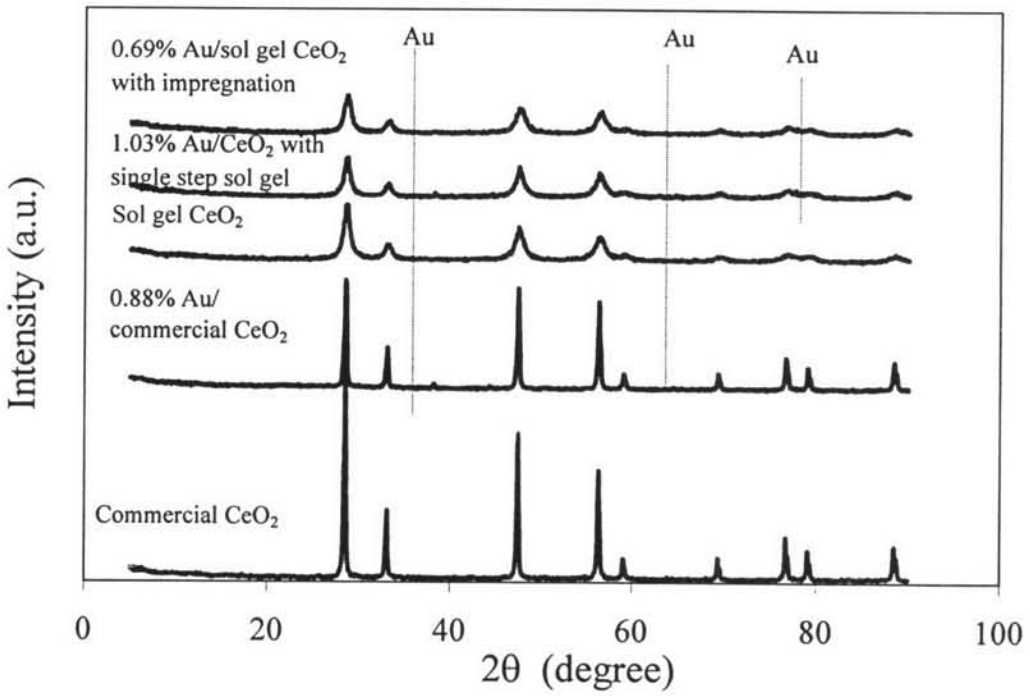

Figure 4.38 XRD patterns of Au/CeO_2 catalysts prepared with different methods compared to that of the pure CeO_2 support.

there was no any dominant peak of gold. The explanation is that all samples contained very low gold contents and XRD cannot detect metal particles smaller than 3-5 nm. Therefore, it can suggest that the size of Au particles on all studied catalysts should not be larger than 5 nm. The crystallite sizes of CeO_2 calculated by Scherrer equation and the BET surface areas of all catalysts are shown on Table 4.4. The results show that, for both commercial CeO_2 and single step sol gel CeO_2, the incorporation of gold during preparation may suppress the growth of ceria crystallites during the calcination step which is in a gold agreement with literature (Qi Fu *et al.*, 2001). The BET results also show that the surface area also decrease in the presence of gold for both commercial and single step sol gel CeO_2. The explanation will be further given in the next section.

Table 4.4 Physical properties of Au/CeO_2 catalysts

Catalysts	CeO_2 mean crystallite size, Å	BET surface area, m^2/g
Commercial CeO_2	369	7.4
0.88% Au/commercial CeO_2	334	6.5
Sol gel CeO_2	131	122
0.69% Au/ sol gel CeO_2 with impregantion	108	113
1.03% Au/CeO_2 with single step sol gel	154	114

As described earlier, the morphology of Au/CeO_2 catalysts is depended upon a preparation method. The SEM morphology of the commercial CeO_2 (with a low BET surface area of 7.4 m^2/g) shows globular particles with rough surface (Figure 4.39 (a)), while the morphology of sol gel CeO_2 is like-needle shaped (Figure 4.39 (b)). The BET surface area of the sol gel CeO_2 is around 122 m^2/g because of the micro-porous structure as depicted in Figure 4.39 (b). The surface morphology of 0.88% Au on the commercial CeO_2 is still similar to that of the pure commercial CeO_2 as shown Figures 4.39 (a) and 4.39 (c). In the case of the sol gel CeO_2 support, the physical shape of the particles does not change when gold is added either via the single step sol gel or via the impregnation method (Figures 4.39 (d)-(e)). For the sol gel CeO_2 support, the needles are around 5-10 μm long. There are several shapes of the sol gel CeO_2 because of the incomplete hydrolysis of CeO_2 during the preparation step.

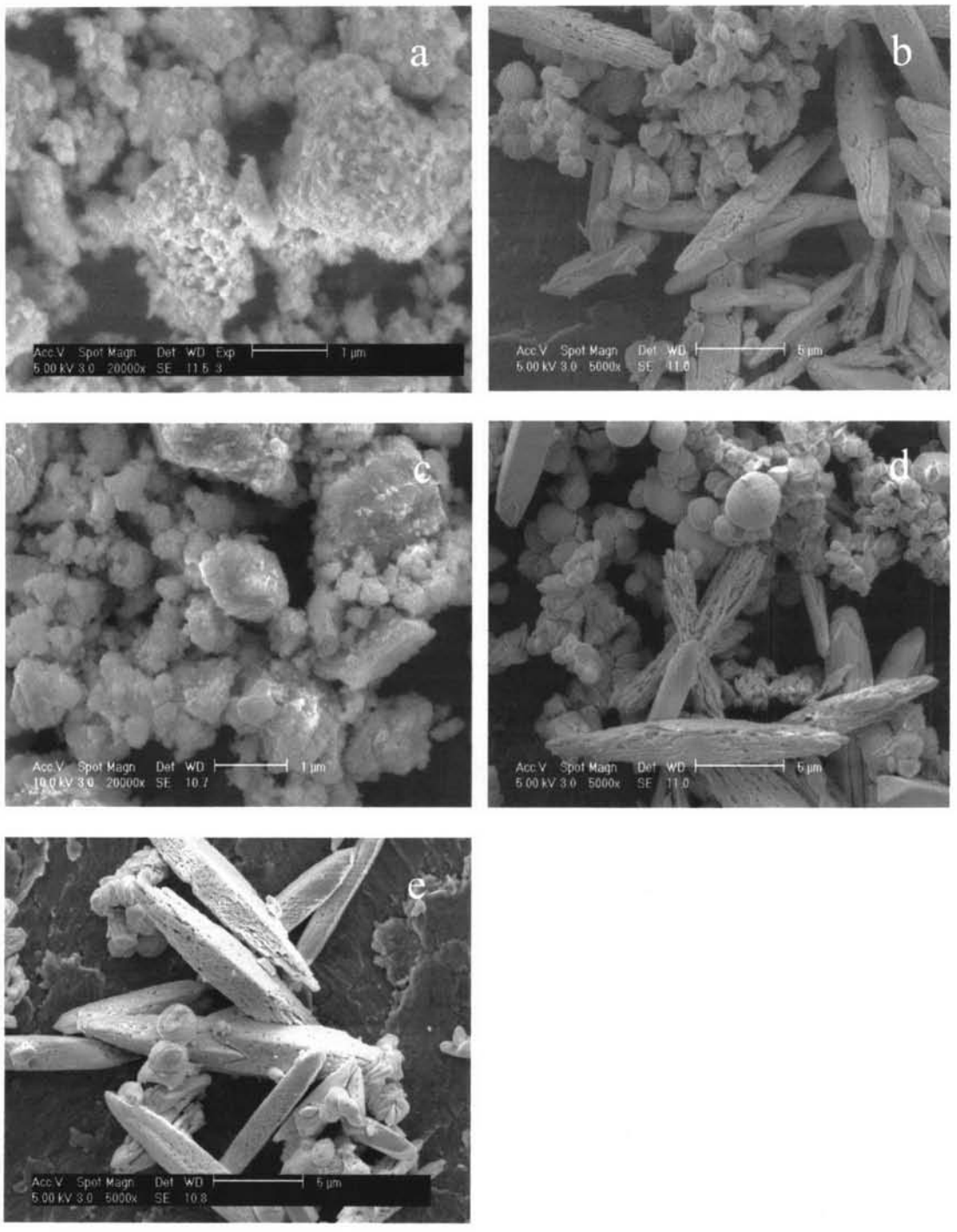

Figure 4.39 SEM surface morphology of (a) commercial CeO2; (b) CeO2 sol gel; (c) 0.88% Au commercial CeO2; (d) 1.03% Au/CeO2 with single step sol gel; (e) 0.69% Au/ sol gel CeO2 with impregnation.

Figures 4.40-4.42 show the transmission electron micrographs of the gold/cerium oxide catalysts with different preparation methods. As be seen from the figures, the high contrast regions on the surface of the CeO_2 particles were identified as gold particles by EDS. In comparisons between the two preparation methods for Au catalysts on CeO_2, the impregnation technique gave a very poor distribution of Au particles on CeO_2. The average gold particle size on the commercial CeO_2 was 1.8 ± 0.5 nm while that on the sol gel CeO_2 with impregnation was 6.2 ± 2.1 nm. As expected, the single step sol gel technique was found to provide a good distribution of gold with an average gold particle size of 5.6 ± 1.5 nm. The higher the dispersion of gold particles, the higher interaction between the Au particles and the CeO_2 support is.

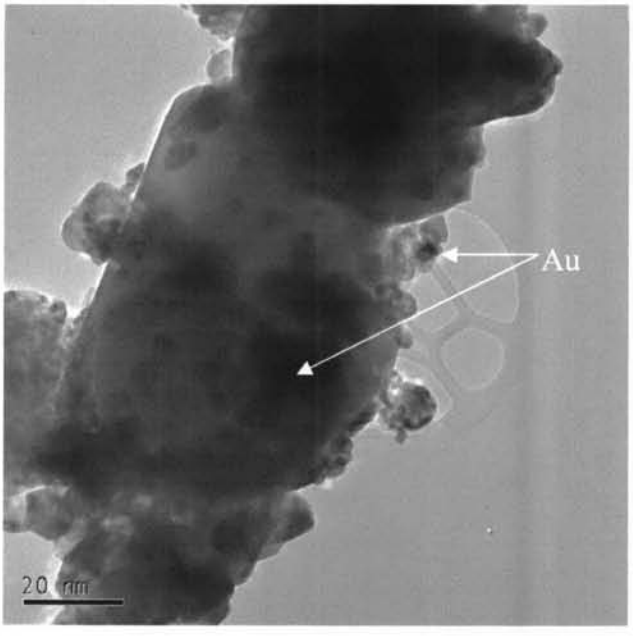

Figure 4.40 Gold particles (dark spots) on the surface of 0.88% Au/commercial CeO_2.

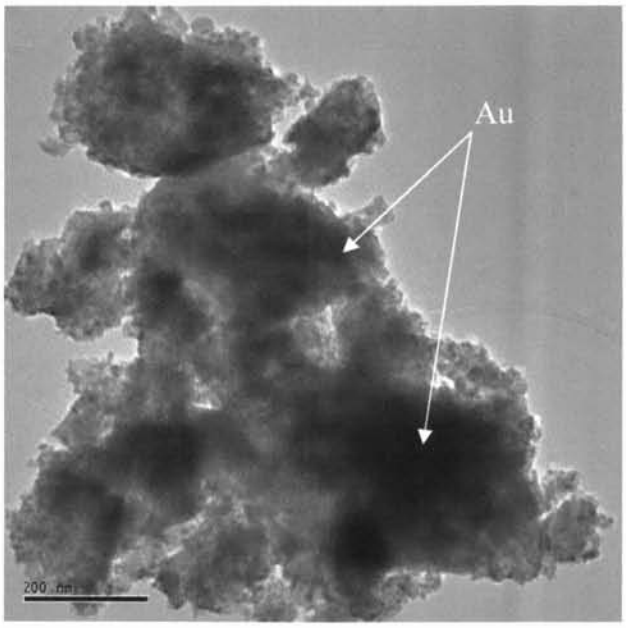

Figure 4.41 Gold particles (dark spots) on the surface of 0.69% Au/ sol gel CeO_2 with impregnation.

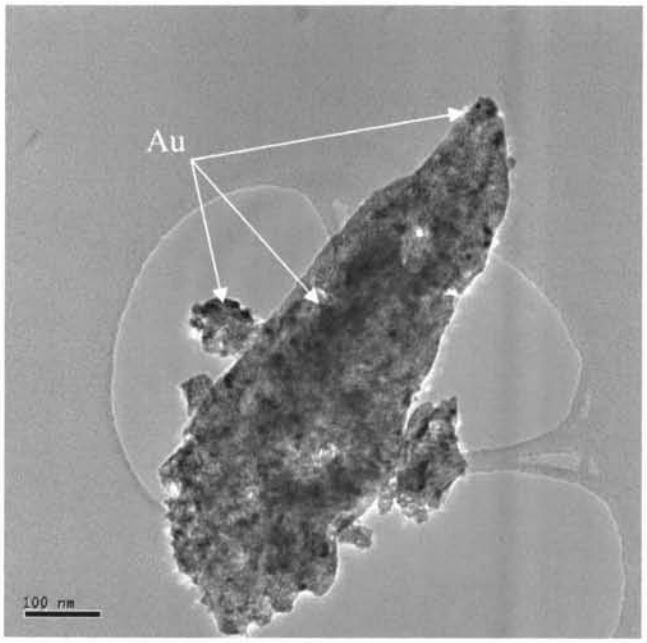

Figure 4.42 Gold particles (dark spots) on the surface 1.03% Au/CeO_2 with single step sol gel.

4.4.2 Catalyst Activity of Ethylene Epoxidation

The activity results of ethylene epoxidation over Au on CeO_2 catalysts with different methods of preparation are summarized in Table 4.5. In comparisons among three catalysts, for any given temperature, 0.88% Au/commercial CeO_2 gave the lowest ethylene conversion and the highest ethylene oxide selectivity. For any given catalyst, the ethylene conversion increased with increasing reaction temperature but ethylene conversion still remained lower than 1%. One may speculate that the small gold particle size (around 1-2 nm) of this catalyst attributes to the low activity for ethylene epoxidation results. It is very surprising that both 1.03% Au/ CeO_2 with single step sol gel and 0.69% Au/ sol gel CeO_2 with impregnation required lower temperatures (140°-200°C) than the Au/CeO_2 (220°-270°C) for both ethylene conversion and the ethylene oxide reaction. The activities of both catalysts are relatively higher but the ethylene oxide selectivity was still low, especially for 0.69% Au/ sol gel CeO_2 with impregnation which catalyzes primarily deep oxidation. Interestingly, 1.03% Au/ CeO_2 with single step sol gel catalyst could produce ethylene oxide in a low temperature range of 140°-180°C, but still gave a low ethylene oxide yield which may be due to either the effect of Au particle size or CeO_2 support. As be known, gold particles larger than 10 nm can catalyze toward the deep oxidation instead of the partial oxidation. However, the gold particle sizes for both catalysts were found less than 10 nm, as confirmed by the TEM results. Therefore, adding gold on CeO_2 does not promote the partial oxidation but predominately produces more CO_2 and H_2O due to the high oxygen mobility of CeO_2 (Hayashi *et al.,* 1998). Oxygen atoms can easily migrate from the bulk to the surface of the CeO_2 support. Therefore, the oxygen molecules on gold active sites can easily dissociate to the CeO_2 support, leading to more atomic oxygen available for the enhancement of deep oxidation. Another possible mechanism is the further oxidation of ethylene oxide due to the high availability of atomic oxygen available on the support surface.

Table 4.5 The catalytic activity of ethylene epoxidation over Au/CeO_2 catalysts prepared with different methods at O_2:C_2H_4=1:1 and different reaction temperatures

Catalysts	Temp. (°C)	C_2H_4 conv. (%)	EO sel. (%)	EO yield (%)
0.88% Au/ commercial	220	0.23	85.93	0.20
CeO_2	240	0.42	82.11	0.35
	255	0.34	55.39	0.19
	270	0.65	63.53	0.41
1.03% Au/CeO_2	140	0.54	76.57	0.41
with single step sol gel	160	0.90	50.96	0.46
	180	1.14	17.96	0.20
	200	2.64	0.00	0.00
0.69% Au/ sol gel CeO_2	140	0.72	54.88	0.40
with impregnation	160	1.22	0.00	0.00
	180	2.11	0.00	0.00
	200	4.33	0.00	0.00

The presence of ethylene oxide was confirmed by the subsequence reaction detected with mass spectrometry as shown in Figure A.3 and Appendix A. DRIFTS reaction was employed to prove ethylene oxide produced over catalysts as shown in Figure 4.43. The reaction was carried out catalyst at 140°C with continuous flow of different gases and the FT-IR spectra were collected after 30 min. These bands are compared with spectra containing epoxy functional groups (800-1300 cm^{-1}) and CH-bending (1300-1600 cm^{-1}) (Skoog *et al.*, 1998). Thus, it can be concluded that each catalyst over DRIFT reaction is ethylene oxide. Moreover, small spectra bands of CO_2 at 2330 and 2360 cm^{-1} are only observed for the 0.69% Au/CeO_2 sol gel with impregnation only.

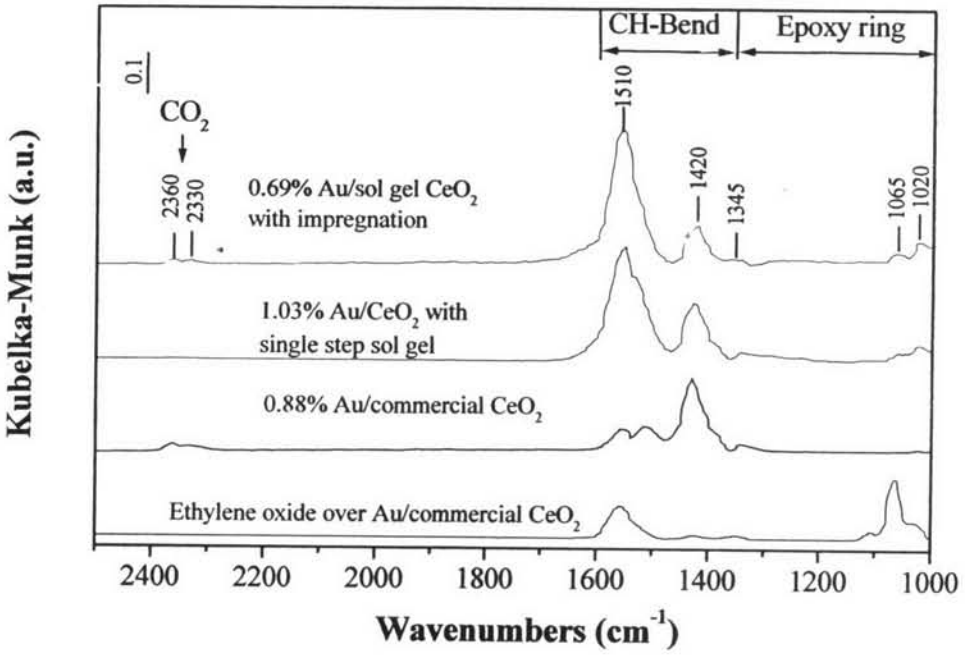

Figure 4.43 DRIFTS spectra of the Au/CeO_2 samples recorded after 30 min exposure at the concentration ratio of $C_2H_4:O_2 = 2\%:2\%$.

4.4.3 Conclusions

In conclusion, all Au/CeO_2 catalysts are not a good catalyst for ethylene epoxidation. Since they gave both ethylene conversion and ethylene oxide yield even though the gold particle size was relatively large (6 nm). The reason is that the interaction between gold and CeO_2 support does not enhance the adsorbed molecular oxygen species, in contrast to the case in Au/TiO_2 catalysts. The oxygen storage property of CeO_2, and its high oxygen mobility facilitate the deep oxidation. Moreover, the TPD result reveals that desorbed oxygen comes from the adsorbed oxygen on the Au site, the adsorbed oxygen on the support surface and the oxygen from the CeO_2 support itself. According to the reaction result, these catalysts provided relatively low activity of epoxidation as compared to the previous study on monometallic Ag and bimetallic Au-Ag catalysts. The presence of ethylene oxide was confirmed by FT-IR spectra.